THE UNIVERSITY OF CHICAGO

PHOTOTHERMAL HEATING TO EXPLORE THE SPATIAL DYNAMICS OF TWO REACTION SYSTEMS

A DISSERTATION SUBMITTED TO

THE FACULTY OF THE PRITZKER SCHOOL OF MOLECULAR ENGINEERING

IN CANDIDACY FOR THE DEGREE OF

DOCTOR OF PHILOSOPHY

BY

TIMOTHY MCCORMICK STEEVES

CHICAGO, ILLINOIS

AUGUST 2020

Acknowledgements

First, I would like to express my sincere gratitude to my advisor Professor Aaron Esser-Kahn for the guidance, support of my research, and allowing me the freedom to explore beyond my research to identify my calling as a scientist. It's been a very long journey, involving more cross-country moves than I was expecting, but I couldn't have asked for a more supportive advisor for my PhD, and I'm so excited to see the Esser-Kahn Lab continue to grow and succeed.

I also want to thank the members of my committee, Professor Alex High and Professor Stuart Rowan, for their insight and encouragement. I trust that they are there to ask the hard questions and make this thesis the best it can be.

My sincere thanks also goes to Professor Rachel Steinhardt, who was an incredible help to me in my years at Irvine, and especially for her help completing the methyl acrylate experiments after I became sensitized to the material.

I also want to thank my labmates, who have been a constant source of insight and support. In particular; Kyle Brubaker, Alfred Chon, Sophia Huang, Seong-Min Kim, Flora Kimani, Hemakesh Mohapatra, and Brittany Moser. All of whom who were sources of great comfort at different points in my PhD.

Finally, I would like to thank my mother, father, step-father, and my sister; all of whom have provided immense emotional support in their own unique ways. Love you all.

Abstract

Illumination of nanoparticles causes "photothermal heating", where the particles heat up faster than they diffuse heat into the local environment, creating a temperature gradient between the particle and the bulk system. When used to drive chemical reactions, it's an example of how simple spatial differences in reaction set-up can alter the macroscale behavior of systems. In the presented work, I have explored photothermal heating in solution as well as in the gas phase to perform high-temperature reactions that normally require that the bulk system be heated. The first is a radical polymerization, where we chose the thermal decomposition of benzoyl peroxide as our target reaction. We demonstrated that this reaction could be done without heating the bulk system. We also saw that the unique reaction geometry of photothermal heating resulted in morphological differences in the resulting polymer. The second reaction explored was the heterogeneous catalyst conversion of carbon dioxide to methane on nickel. Using nickel nanoparticles and light as both the catalysts and heat source, we were able to perform these reactions well below the usual bulk temperatures required, and below even what is used for supported photothermal catalysts. Finally, we extended our exploration of spatial systems to two other systems and used finite element modeling to complement reaction and system design.

Table of Contents

Table of Figures

Table of Images

Table of Tables

Introduction & Background

Our initial exploration was based on the following question: Could the photothermal heating of nanoparticles be used to drive chemical reactions that require higher temperatures, and if so, how intense was the effect? This guided our exploration of utilizing carbon black nanoparticles to drive the decomposition of benzoyl peroxide for radical polymerization and allowed us to estimate an "effective" temperature of the nanoparticles under the reaction conditions we tested it in.

After this success, I wanted to explore more ambitious ideas and target industrial reactions where the temperature management of the system is the limiting factor in the industrial efficiency. We targeted the Sabatier reaction and asked two question: Can this high-temperature reaction be driven solely from photothermal nanoparticles? And: Could these same nanoparticles act as the necessary catalyst? The bulk of my work in the past three years has been focused on this issue.

There have also been several instances of assistance on other projects as well, exploring spatial relationships of a microfluidic system as well as a dynamic polymer system. Though not directly related, the thread tying all these projects together is a simple, spatial approach to a wide variety of problems. By identifying new ways to do reactions, we can significantly expand the toolkit we use to perform chemical transformations.

As a disclaimer, I will note that material in this background has been reproduced and adapted from the relevant publications, including my master's thesis and two presubmission manuscripts.

1.1 Carbon Capture and Conversion

I am very passionate about working on renewable energy research, and part of what drew me to this lab was the novel was they have focused in on specific optimization for parts of the industrial process. I ended up focused on one important aspect of renewable energy research; releasing CO_2 from capture solutions.

Right now, we make most of our energy from fossil fuels, releasing CO_2 into the air. Previously, we released all sorts of toxic byproducts of combustion, but thanks to innovations in capture and catalytic conversion most of the most toxic elements are neutralized. Nitrogen emissions for example are way down due to a combination of separations and conversions processes. So, the question has emerged, why can't we do that for CO_2? We now know that greenhouse gases are severely affecting our climate, so if we could remove carbon dioxide from our flue gas, we would solve our problem—no more greenhouse gas exhaust from fossil fuel combustion.

1.1.1 Carbon Capture

Despite the appeal of carbon capture, it's use is currently very limited. There are two main reasons driving this. The first is that there's too much of it to just store

indefinitely, it needs to go somewhere or be converted into something. The second is that it's energy intensive. You have to remove the carbon dioxide from the flue gas stream, reducing the efficiency of your power plant for no short-term gain. These are the core issues holding back the implementation of carbon capture and sequestration.

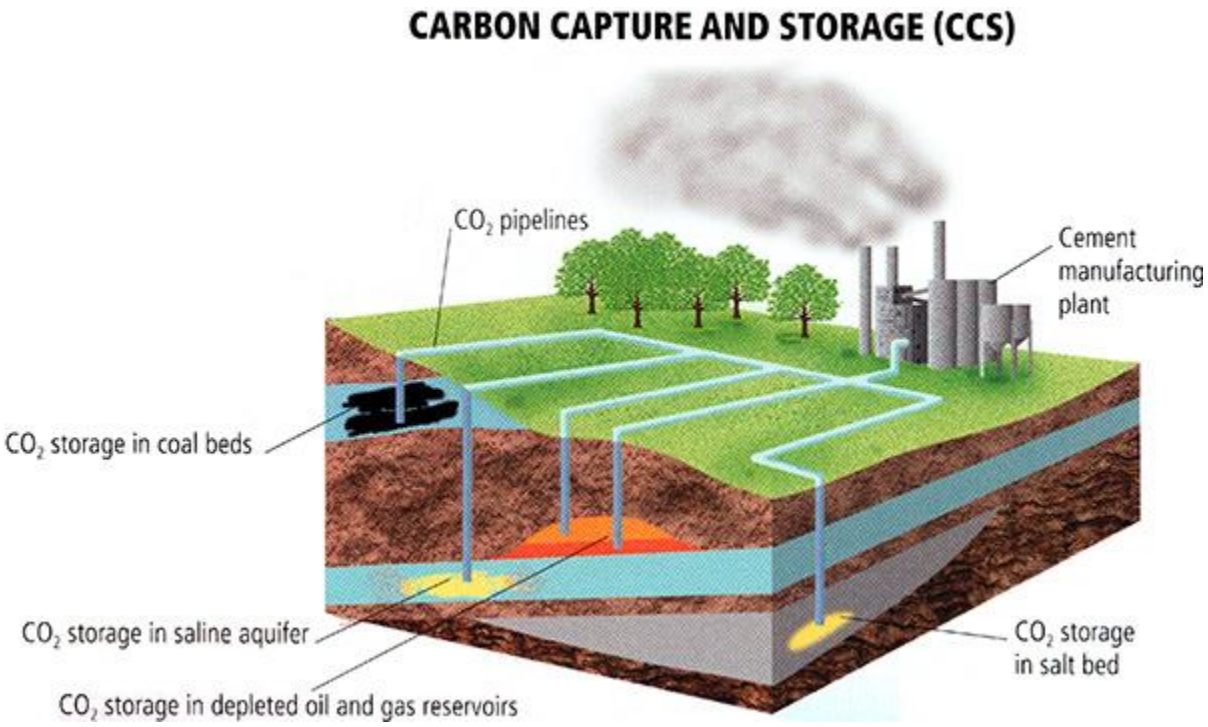

Figure 1: Carbon Capture and Sequestration (CCS) illustrative diagram from Dire Predictions: Understanding Climate Change[1]

Capture solutions are often amine-based systems that flue gas bubbles through, and the CO_2 binds to the nitrogen in the amine groups[2]. These work great at capturing the CO_2, but then it's stuck there, so it must be heated to release the gas into whatever

[1] Mann and Kump, *Dire Predictions*.
[2] Dutcher, Fan, and Russell, "Amine-Based CO2 Capture Technology Development from the Beginning of 2013—A Review."

compressor or container is the next step in the project. And because many of these systems are water based or have some other solvent system, heating of the entire system is very energy intensive[3].

Our lab's novel idea was to photothermally heat nanoparticles to do this part of the separation, specifically carbon black. Once gas is released and escapes the solution, the reaction is irreversible, so the particles can pull the gas out of solution, have it bubble out, and restart the process. This was an ideal application of our system, and part of what drove us to explore other reaction systems that had equilibrium shifts based on heat.

1.1.2 Conversion and Solar Fuel

Solar fuel refers to chemical fuel that was generated using the energy harnessed from the sun. The dream of solar fuels is that you could make them out of the captured CO_2 we were talking about earlier, burn them, then capture the CO_2 from that and repeat the process. If you use the sun for all or most of the energy throughout the whole process, you're basically storing the energy from sunlight into those chemical bonds inside the fuel. This is excellent for the widespread use of renewable energy, since fuel

[3] Leung, Caramanna, and Maroto-Valer, "An Overview of Current Status of Carbon Dioxide Capture and Storage Technologies."

is easier to store, denser, and more versatile than any battery[4]. The scientific problem then, is optimizing each step of the process and using sunlight to drive it, which is what I focused the core work of my thesis on.

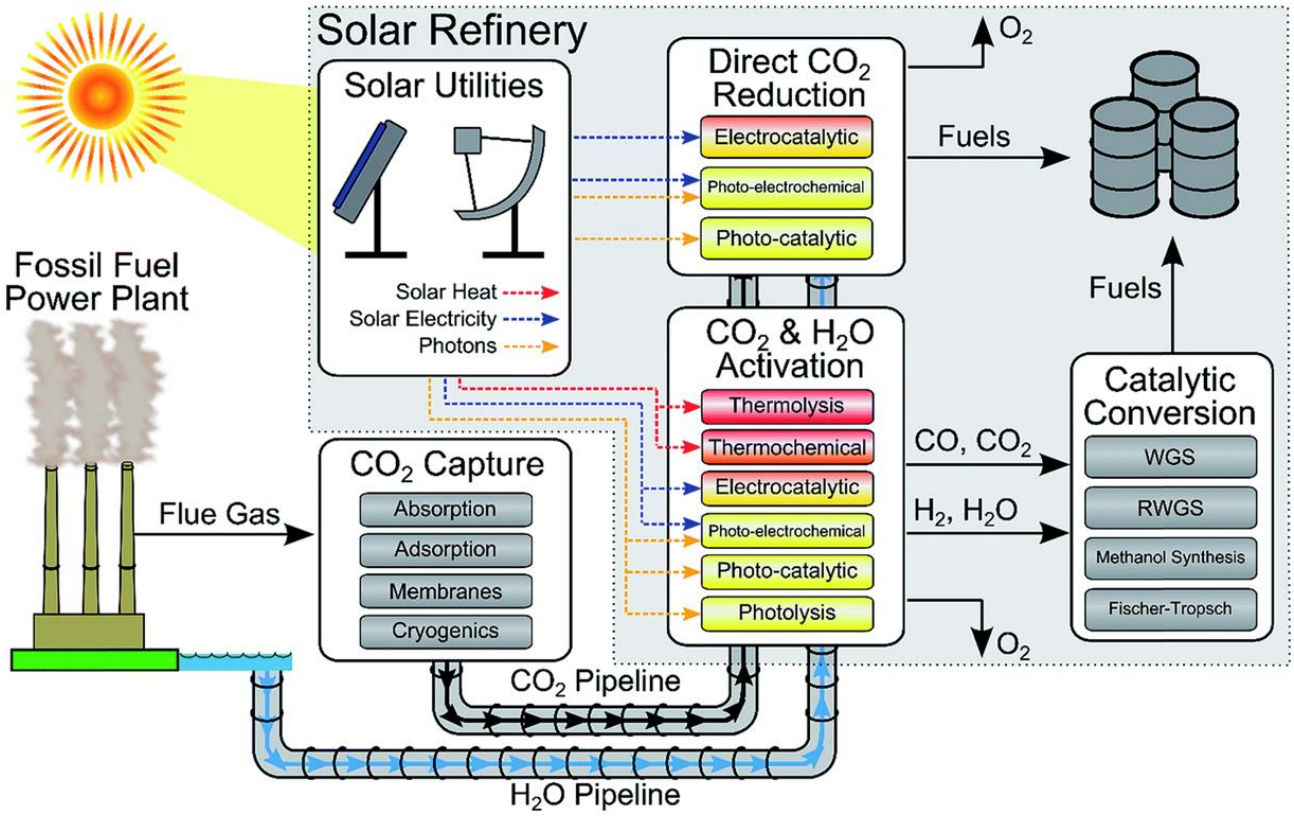

Figure 2: A flowchart-style diagram that illustrates the many separations and chemical processes that could be involved in a solar refinery system.[5]

[4] Scott Dial, "Selected Energy Densities Plot."
[5] A. Herron et al., "A General Framework for the Assessment of Solar Fuel Technologies."

1.2 Nanoparticles and Photothermal Heating

Nanoparticles are a class of matter defined by their size. They are (usually) spherical particles ranging in size from 1 nm to 1 μm. Matter in this space range straddles the line between large molecules like polymers and bulk materials, and they have found unique functionally in the many fields including optics, medicine, imaging, and energy.

Nanoparticles occur both naturally and are synthesized for a variety of purposes. Plenty of biomachinery (e.g. proteins, RNA, DNA, etc.) can be classified as nanoparticles; all sorts natural occurring minerals come in a form that falls in this category, including moon dust[6]. Most of their interesting properties stem from the fact that they have a high surface area-to-volume ratio. This means that, based on the size of the particle, electronic qualities of the surface atoms can be just as, if not more, important than that of the internal atoms to the overall qualities of the material. This also allows them to dissolve in solutions despite being much bigger than your average solute, since the surface-solvent interactions are so strong.

[6] Cain, "Lunar Dust."

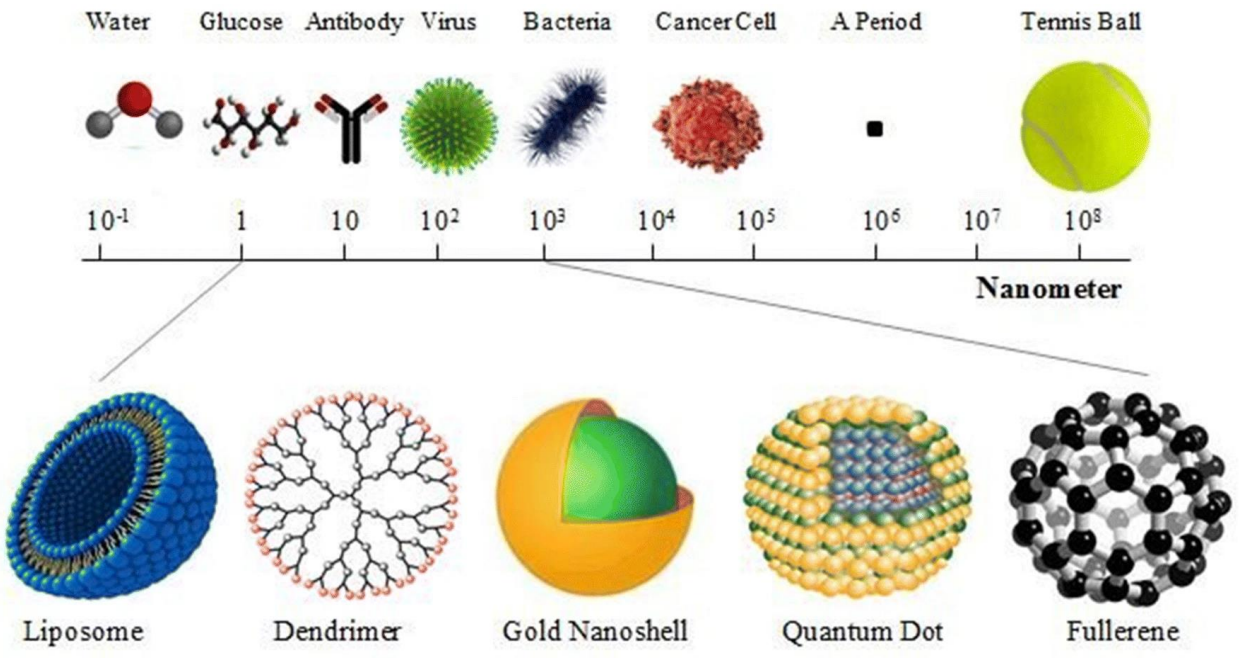

Figure 3: A depiction of the size and diversity of matter of common nanoparticles.[7]

We've been using both natural and synthetic nanoparticles for quite a long time. As shown in image 1, certain metal particles were mixed into the silica used to make glass due to the resulting optical properties, which comes from metal nanoparticles phenomena of plasmonic absorption of light. This is an observable phenomenon this was well characterized centuries ago, but only with modern electrodynamics has it been explained theoretically. Asbestos is another example of natural nanotech, the naturally occurring nanostructured fibers that are still some of the most widely used nanomaterials. Both their usefulness as a flame retardant and their long-term carcinogenicity are due to their nanostructured nature.

[7] Raj K. Keservani and Anil K. Sharma, *Nanoparticulate Drug Delivery Systems*.

Most matter heats up when it absorbs light, and nanoparticles are just matter of a certain size. Due to this size the rate at which nanoparticles absorb energy in relation to how quickly they can disperse that energy to their surroundings can be unbalanced enough to create a nonequilibrium state, where particles and their surroundings always remain much hotter than the bulk solution.

Photothermal heating is the result of particles rapid heating from illumination being higher than the rate of dissipation to the environment. This unique set of properties can drive all sorts of thermal process such as; melting, heat catalysis, and phase change. What makes the phenomena so useful is that the heat remains localized around the particle. In an initial example of this phenomenon, the Halas group demonstrated that it was possible to boil a whole cup of water at well below 100 °C, using the carbon black to produce steam around each nanoparticle while the bulk solution remained at 40 °C[8]. In addition to steam generation, research has focused on using photothermal heating for drug delivery, targeted pyrolysis in the body, and the focus of chapter 3, catalysis[9].

---

[8] Neumann et al., "Solar Vapor Generation Enabled by Nanoparticles."

[9] Chen et al., "Targeting of Pancreatic Cancer with Magneto-Fluorescent Theranostic Gold Nanoshells"; Sershen, Halas, and West, "Pulsatile Release of Insulin via Photothermally Modulated Drug Delivery"; Hirsch et al., "Targeted Photothermal Tumor Therapy Using Metal Nanoshells"; Swearer et al., "Plasmonic Photocatalysis of Nitrous Oxide into N2 and O2 Using Aluminum–Iridium Antenna–Reactor Nanoparticles"; Zhou et al., "Light-Driven Methane Dry Reforming with Single Atomic Site Antenna-Reactor Plasmonic Photocatalysts."

Image 1: Stained glass in Rockefeller Chapel at the University of Chicago, photo credit to Quinn Dombrowski

One of Richard Feynman's many contributions to science was the popular lecture "There's Plenty of Room at the Bottom", which elaborated and explored what might be possible as explored physics at smaller and smaller scales[10]. Contrary to popular belief, it was not the inspiration for the explosion of nanotechnology research we have seen in the last 40 years, but it referred to as a prescient observation, and reads quite appealingly[11].

The two sets of particles I use in my work are carbon black nanoparticles and nickel nanoparticles. Carbon black is essentially ultrafine soot, generated by incomplete

[10] Feynman, "Plenty of Room at the Bottom."
[11] Chris Toumey, "Apostolic Succession."

combustion of carbohydrates to form amorphous carbon spheres[12]. Industrially it is used in dyes to color things black and as an additive in many materials, such as rubber, to strengthen the material. It's also, as the name might indicate, very black. It absorbs almost all the solar spectrum very well, making it a great way to turn sunlight directly into heat[13]. It's also very inexpensive, which makes it a compelling prospect for proposed industrial use over many other forms of carbon nanomaterials, which often cost significantly more to produce.

Metal nanoparticles often heat via plasmonic resonance, which is a specific way of converting light to heat using the free electrons of metals. The most common example in the literature is gold, which absorbs at very specific wavelengths due to plasmon resonance[14]. The physics will be discussed directly in the next section, but essentially these particles absorb a very particular wavelength of light very well, which is dictated by their size, geometry, and material. Illuminating them at this wavelength makes them absorb the energy with their electron cloud, where the then excited plasmon will relax out of its excited state via thermal relaxation, generating heat. The "plasmons" of plasmonic absorbance also can be utilized to do stuff beyond heating, as the absorbance mechanism involves some usually high excitation states which can be carefully tuned.

---

[12] Donnet and Voet, *Carbon Black*.
[13] Han et al., "Thermal Properties of Carbon Black Aqueous Nanofluids for Solar Absorption."
[14] Li and Gu, "Gold-Nanoparticle-Enhanced Cancer Photothermal Therapy."

All metal nanoparticles will do this to a certain extent, but important to our discussion is to note that nickel does far less than gold, silver, or copper[15]. We make use of the broad-spectrum absorption of nickel, using it like a carbon black that could also serve as a catalyst.

1.2.1 Plasmonic Heating and Bulk Absorption

Plasmonic nanoparticle heating encompasses much of what has been published on regarding photothermal nanoparticles. It's very useful in medical systems because the particles can be activated selectively with a laser directed to the point of therapy, be that a tumor, adipose tissue, or anywhere else you want the particle to heat up and release a drug, kill cells, or inducemetabolic changes[16].

Plasmons are quanta of oscillations in plasma, which in this case refers to that "sea of electrons" that are freely distributed in a metal. The characteristic plasmon frequency of bulk metal determines at what light ranges it is reflective and what ranges it is transmitted. This property is why most metals are reflective and colorless. Surface plasmons are these oscillations at the surface of the material, where the sea of electron ends and the reaction and coupling to outside forces is strongest. Surface plasmons are especially important to the nanoparticles, since they are more surface property-

---

[15] Chen et al., "Plasmonic Nickel Nanoantennas."
[16] Khlebtsov and Dykman, "Optical Properties and Biomedical Applications of Plasmonic Nanoparticles."

dependent than most materials. The plasmonic resonance effect is when the surface plasmon resonates with the photons of light. All of this requires a specific wavelength for the optimal absorbance, so we opted instead for bulk absorption.

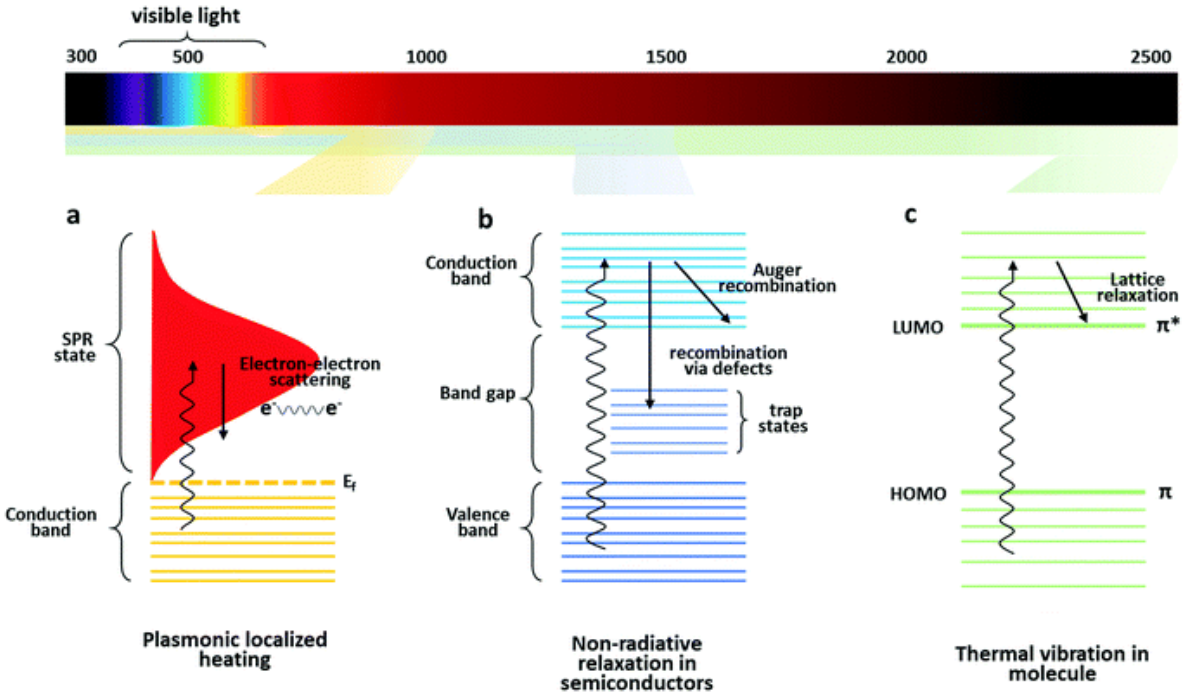

Figure 4: Figure depicting the different ways heat is absorbed by physical matter and converted into heat. From Gao et al.[17]

Carbon black, as previously mentioned, is soot from incomplete combustion. It absorbs across the solar spectrum. Nickel has a similarly broad absorption, due to a limited plasmon resonance effect.

[17] Gao et al., "Solar Absorber Material and System Designs for Photothermal Water Vaporization towards Clean Water and Energy Production."

Figure 5: Carbon Black, open domain image

Carbon black, carbon nanotubes, and other various broad absorbers are often talked about without differentiating their light absorbance mechanism. This is not accurate, as plasmonic resonance plays no part in the absorbance. Rather carbon black is composed of a dense carbon network that's excellent at absorbing across the solar spectrum[18]. They are also highly conductive, for related reasons.

[18] Donnet and Voet, *Carbon Black*.

1.2.2 In Solutions and Solids

One application of photothermal heating is low-temperature distillation. The particles heat up so fast they vaporize the solvent around them and form a vapor bubble jacket. This bubble jacket flows upward due to buoyancy and is deposited at the surface. Any heat-based reaction in solution that releases gas can do the same. Back in 2014, our lab showed we could use carbon black to pull CO_2 out of CO_2 capture solutions, which is energy intensive separations work that affects the energy efficiency of carbon capture technology[19]. This same thing can be done in solids, such as ice[20]. Since the particles are more fixed, it's more about changing the properties of the material than getting anything out of it, but you can quickly remold something by shining light on it and making the material melt temporarily.

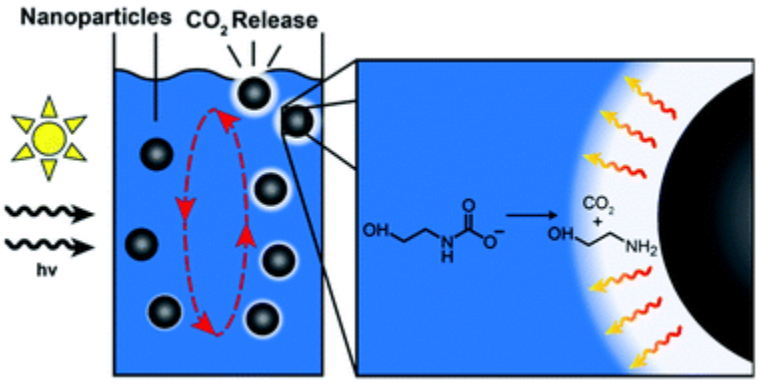

Figure 6: CO_2 release from capture solutions via photothermal heating of carbon black[21]

[19] Nguyen et al., "Photothermal Release of CO2 from Capture Solutions Using Nanoparticles."
[20] Richardson et al., "Thermooptical Properties of Gold Nanoparticles Embedded in Ice."
[21] Nguyen et al., "Photothermal Release of CO2 from Capture Solutions Using Nanoparticles."

The mechanism by which this occurs in solution is still discussed and comes down to two transport-based systems. The first is the nanobubble hypothesis, that the localization of heat around the particle is so great that the particle superheats and a jacket of gas forms around it, further insulating the particle from heat diffusion[22]. Thus, the only heating that occurs is on water that undergoes a phase transition, and the rest of the water the system remains almost unheated[23]. The ideal formation of this hypothesis requires such rapid heating that the intensity of the light required is much too high to be practical for solar applications. The second hypothesis is simply that this is standard bulk heating, where the particles don't vaporize any gas until the bulk temperature of the system reaches boiling. This is much more reasonable to achieve under standard solar illumination. The reality is that both mechanisms seem to be true, bulk heating occurs until the rate of heating outstrips the rate of heat diffusion. The details depend on the peculiarities of the system, but what was compelling about the nanobubble hypothesis still occurs, just with some bulk heating occurring before it's possible.

Our lab has applied this principle in CO_2 release from capture solutions. Where the solution is usually heated in order to get the gas to be released from the capture

[22] Jones et al., "Ultrafast Modulation of Thermoplasmonic Nanobubbles in Water."
[23] Neumann et al., "Solar Vapor Generation Enabled by Nanoparticles."

system[24]. In these experiments the transport kinetics seemed to favor nanobubble formation, which makes sense, as the formation of gas was a reaction as opposed to a phase transition. This success was what inspired us to attempt other reactions with photothermal heating that would cascade into larger changes in the overall system, such as radical polymerization.

1.2.3 Relevant Examples

The Halas group deserves recognition for their work identifying and refining applications for photothermal heating. They've shown numerous applications in the medical field, including targeted hyperthermal therapy for cancerous tumors[25] and photothermally triggered drug delivery[26]. They've also done extensive work in desalination and distillation[27], investigated plasmon-driven photocatalysis[28], and

---

[24] Dutcher, Fan, and Russell, "Amine-Based CO2 Capture Technology Development from the Beginning of 2013—A Review."
[25] Chen et al., "Targeting of Pancreatic Cancer with Magneto-Fluorescent Theranostic Gold Nanoshells"; Ayala-Orozco et al., "Sub-100nm Gold Nanomatryoshkas Improve Photo-Thermal Therapy Efficacy in Large and Highly Aggressive Triple Negative Breast Tumors"; Cole et al., "Photothermal Efficiencies of Nanoshells and Nanorods for Clinical Therapeutic Applications"; Hirsch et al., "Targeted Photothermal Tumor Therapy Using Metal Nanoshells"; Lal, Clare, and Halas, "Nanoshell-Enabled Photothermal Cancer Therapy."
[26] Sershen, Halas, and West, "Pulsatile Release of Insulin via Photothermally Modulated Drug Delivery."
[27] Neumann et al., "Compact Solar Autoclave Based on Steam Generation Using Broadband Light-Harvesting Nanoparticles"; Neumann et al., "Combining Solar Steam Processing and Solar Distillation for Fully Off-Grid Production of Cellulosic Bioethanol"; Neumann et al., "Compact Solar Autoclave Based on Steam Generation Using Broadband Light-Harvesting Nanoparticles"; Neumann et al., "Solar Vapor Generation Enabled by Nanoparticles"; Alabastri et al., "Resonant Energy Transfer Enhances Solar Thermal Desalination."
[28] Robatjazi et al., "Plasmon-Induced Selective Carbon Dioxide Conversion on Earth-Abundant Aluminum-Cuprous Oxide Antenna-Reactor Nanoparticles"; Swearer et al., "Plasmonic Photocatalysis of Nitrous Oxide into N2 and O2 Using Aluminum–Iridium Antenna–Reactor Nanoparticles"; Zhou et al., "Light-Driven Methane Dry Reforming with Single Atomic Site Antenna-Reactor Plasmonic Photocatalysts."

explored the basic science of photothermal heating[29]. We discuss three of these papers in the following section, as well as another of their papers in the review of current methanation research.

In 2013, the Halas group published their initial exploration of a way to utilize solar energy for steam generation and ethanol distillation[30]. Desalination and steam generation are useful, energy intensive processes that require quite a bit of energy. Desalination is a separations process, and energy intensive to the point that it is not currently a viable way to collect potable water from the environment for most populations. As water scarcity becomes a global concern, lots of interest has been directed towards identifying ways to desalinate more efficiently, including directly harnessing solar radiation to drive the process. The Halas study utilized both commercially purchased carbon black as well as gold-coated silica nanoshells that were developed previously in their lab to have a broad and tunable absorbance[31]. In these experiments they utilized a basic solar concentrator to generate steam within a water nanoparticle solution. This system produced steam even when the system was being held in an ice bath to control for bulk temperature. Further analysis concluded in both

[29] Hogan et al., "Nanoparticles Heat through Light Localization"; Brongersma, Halas, and Nordlander, "Plasmon-Induced Hot Carrier Science and Technology"; Zhou et al., "Quantifying Hot Carrier and Thermal Contributions in Plasmonic Photocatalysis."
[30] Neumann et al., "Solar Vapor Generation Enabled by Nanoparticles."
[31] Brinson et al., "Nanoshells Made Easy."

cases that the energy from sunlight was being converted to steam at 80% efficiency, meaning only 20% was lost to heating the bulk water. When distilling ethanol, they were able to do something very similar, except with their ethanol distillate thy broke the water-ethanol azeotrope barrier, producing up to 99% ethanol fractions. These experiments clearly involved the formation of a nanobubble, since they produced vapor and suggested that the macroscopic models of bubble formation may not sufficiently explain the system, and the non-equilibrium temperatures and pressures around the nanoparticle would need to be further explored. And they related a reasonable theoretical exploration of how the density might affect steam generation. Many other papers have explored photothermal evaporation since then, and **Figure 7** illustrates the many different approaches that have been taken.

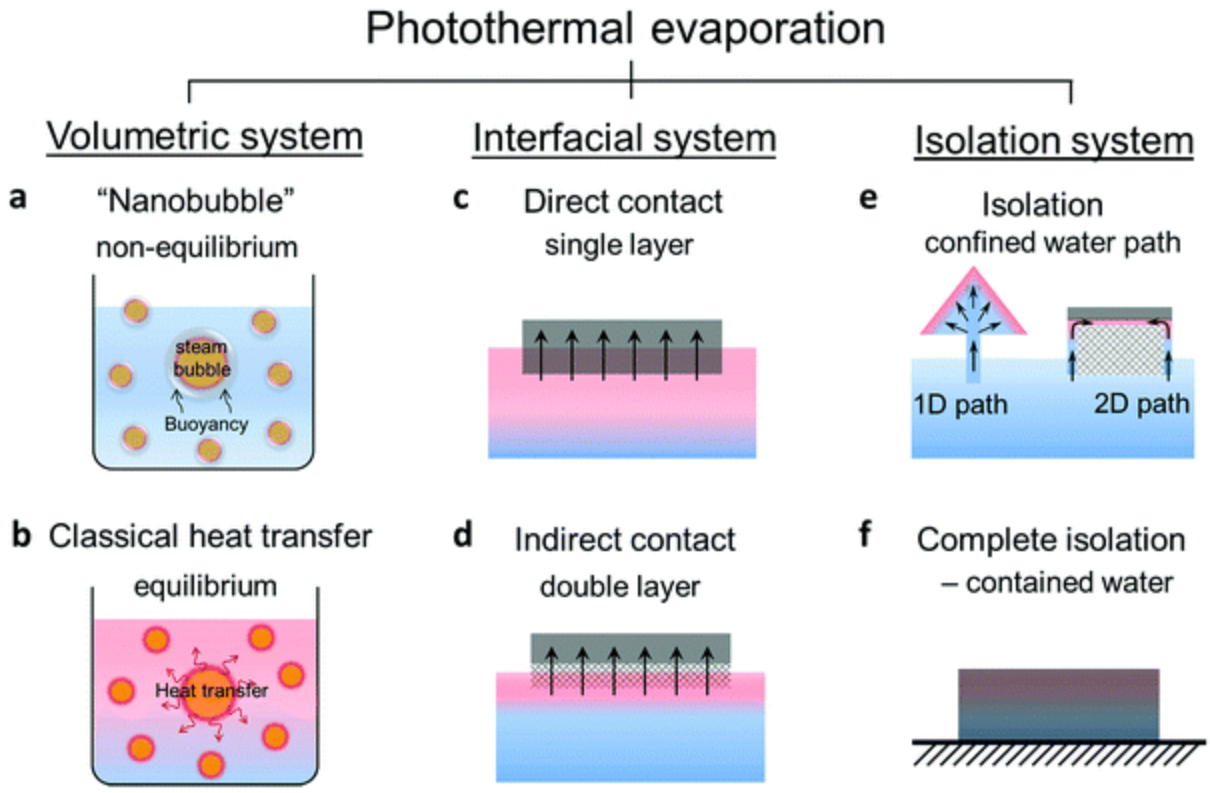

Figure 7: From Gao et al.[32] Shows the different reaction geometries that can be used for solar-driven photothermal evaporation

Drug delivery is another important application of photothermal heating. In 2003, the Halas group published a paper detailing their work using gold nanoshells to release insulin from a biogel for near-infrared light-activated insulin release[33]. In this paper the polymer was bonded to the nanoshell, which was tuned to respond to near-infrared light. This form of light can penetrate tissue well but it also not harmful and is often used in laser therapy. The resulting system can control the release of insulin through

[32] Gao et al., "Solar Absorber Material and System Designs for Photothermal Water Vaporization towards Clean Water and Energy Production."
[33] Sershen, Halas, and West, "Pulsatile Release of Insulin via Photothermally Modulated Drug Delivery."

short pulses, allowing for adjustment based on the amount of time the particles are irradiated.

The final paper from Halas is one in which they examined how plasmonic nanoparticles might affect photocuring epoxies[34]. They examined how laser curing of epoxy films altered the properties of the resulting films, based on if they were doped with nanoparticles, and if so, how much. They found that the process deviated based on if the nanoparticles were present. They identified a multistage process where the nanoparticles first cured the volume around them, and then the particles and the laser heated the rest of the material high enough for bulk curing. The resulting polymer was much stronger than via laser or heat curing alone, and when used to bond two materials, created a bond stronger than any of the components. This illustrates the unique ways in which spatial manipulations of reactions via nanoparticles can produce unexpected results.

1.3 Free Radical Polymerization

Free radical polymerization is a chain growth polymerization where a radical is generated and grows a chain through an iterative reaction with the growing chain and monomer. It's how we make most acrylics and Styrofoam, among other polymers.

[34] Roberts et al., "Plasmonic Nanoparticle-Based Epoxy Photocuring."

1.3.1 Mechanism

Radical polymerization is driven by the action of radicals on various reactive vinyl groups. The basic reaction scheme for radical polymerization is shown in **Figure 8**. A radical is introduced into a solution which contains a monomer with a reactive vinyl group[35]. The radical combines with one of the vinyl electrons to form a bond and a new radical located on the monomer[36]. This process repeats with the new radical and another monomer until the chain is terminated by reaction with another radical in solution, either another growing chain or a different free radical from the initiator[37]. The process can be performed in a solvent, as an emulsion-based polymerization, or as a bulk polymerization with no solvent[38]. Radicals can be generated in numerous different ways. Commonly they are generated from either heat-based or light-based decomposition of an initiator[39]. In our experimentation, we focused exclusively on the thermal initiator benzoyl peroxide as our radical source.

---

[35] Odian, *Principles of Polymerization*.
[36] Odian.
[37] Odian.
[38] Odian.
[39] Odian.

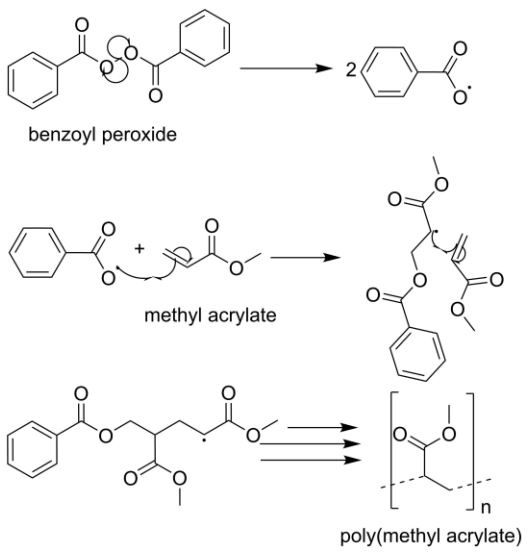

Figure 8. *Schemes depicting the basic process for the free radical polymerization of methyl acrylate. In the first step the initiator, benzoyl peroxide, decomposes into two peroxy radicals which then go on in the following step to react with monomers to create actively growing chains. The final step encompasses the rapid growth and termination steps which the growing chains perform to form the final product polymer chains. At 70° C the half-life for BPO decomposition is 10 hours[40].*

1.3.2 Bulk and Solution Polymerization

The actual reaction being initiated by heat is the decomposition of benzoyl peroxide into two separate peroxy radicals[41]. The bond between the two oxygens in the peroxide cleaves spontaneously and symmetrically at high temperatures[42]. The important feature is the symmetry of the breakage, with one electron going to each oxygen, resulting in two radicals. This reaction is the key in two of our experiments: first to initiate radical polymerization in a bulk monomer solution via nanoscale heating

[40] Co, "Free Radical Initiators."
[41] Barnett and Vaughan, "The Decomposition of Benzoyl Peroxide. I. The Kinetics and Stoichiometry in Benzene."
[42] Barnett and Vaughan.

of carbon black nanoparticles and then on its own within a solution of ethyl acetate to examine the way nanoscale heating alters the reaction kinetics. Benzoyl peroxide was an ideal target for the nanoscale heating because of its well-studied kinetics and high decomposition temperature. Thermal decomposition of benzoyl peroxide doesn't occur significantly at room temperature and occurs at slow, manageable rate even at 56 ^{o}C, the highest temperature we observed in our illuminated carbon black solutions[43]. It is important to mention and highlight that although many radical initiators may be decomposed via visible light, benzoyl peroxide is specifically a thermal initiator, and is not sensitive to visible light.

The two most common ways of initiating a radical polymerization are thermal and light-based initiators. Our system used benzoyl peroxide, a thermal initiator that has no light-based decomposition. However, it is worth briefly discussing how light (often UV light) initiated radical polymerizations differ from their thermal counterpart, as we are investigating ways to use light to drive a heat-based system. For radical polymerization, the only difference is in the initiator decomposition, once the radical is generated the reaction proceeds as previously described. Below is a quote from a review by Kuar and Srivastava; summarizing photopolymerization and it's uses:

[43] "Thermal Initiators: Decomposition Rate and Half-Life."

Photopolymerization, the utilization of electromagnetic radiation (or light) as the energy source for polymerization of functional monomers, oligomers, and polymers, is the basis of important commercial processes with broad applicability, including photoimaging and ultraviolet (UV) curing of coatings and inks. These processes require light that is absorbed by the system and utilized to effect the formation of new chemical bonds: Photoinitiators, photocrosslinking agents, and photocrosslinkable polymers.

> Photoinitiators absorb light in the UV–visible spectral range (250–450 nm) and convert this light energy into chemical energy in the form of reactive intermediates, such as free radicals and reactive cations, which subsequently initiate polymerization of functional monomers to form linear polymers, whereas the multifunctional monomers give three-dimensional crosslinked networks.[44]

The benefits of photopolymerization are that the light intensity and switchable light allows for greater control of the reaction. Our system provides similar benefits but was

[44] Kaur and Srivastava, "Photopolymerization."

not chosen as a replacement for either type of reaction, but rather as an exploration what could be possible with photothermal heating.

As previously mentioned, once the peroxy radicals are formed in solution, they initiate polymerization. This polymerization occurs as chain growth, a process where chains extend rapidly and terminate much more quickly than they are generated, resulting in a reaction solution that is primarily monomer and completed polymer chains at any given moment[45]. As the reaction continues and the composition of solutions becomes more viscous, the chains terminate less rapidly, as the active radical ends of the chains are functionally immobilized by the viscous solution and are therefore unable to react with other chain ends but are able to react with more monomer[46]. This phenomenon results in near-instantaneous completion of the reaction, as numerous immobilized growing chains rapidly consume all the monomer present. An additional feedback loop is present in the form of heat from the exothermic reaction of chain growth. This heat rapidly increases the temperature of the solution, and this in turn increases the rate of the reaction. It can also melt vessels and boil the solution, so caution must be observed, and autoacceleration is often viewed as a dangerous or destructive phenomenon. However, for our purposes, it serves as a highly useful

[45] Odian, *Principles of Polymerization*.
[46] Odian.

endpoint metric. Autoacceleration occurs at a certain degree of conversion each time and puts out enough heat that it's simple to measure. The time it takes the reaction to reach the autoacceleration point is a measure of the generation rate of the radicals.

1.3.3 Literature Examples of Photothermally Driven Polymerization Reactions

Photothermal heating of nanoparticles has been used to drive other polymerization related reactions. In 2015, the Lear group published a paper detailing the use of plasmonic gold nanoparticles to photothermally cure urethane[47]. This urethane system was not suitable to bulk curing, as the bonds formed were weak enough to be degraded by high thermal conditions. Thus, the photothermal heating driven by intense laser light allows for high temperature curing at low bulk temperatures. A similar paper from the group in 2017 showed gold nanoparticles being used to cure polydimethylsiloxane (PDMS)[48]. A follow-up examined the changes to mechanically properties that arose from photothermal curing of PDMS, they identified that tuning the level of light during the curing could alter the properties of the polymer network[49].

---

[47] Haas and Lear, "Billion-Fold Rate Enhancement of Urethane Polymerization via the Photothermal Effect of Plasmonic Gold Nanoparticles."
[48] Fortenbaugh and Lear, "On-Demand Curing of Polydimethylsiloxane (PDMS) Using the Photothermal Effect of Gold Nanoparticles."
[49] Fortenbaugh, Carrozzi, and Lear, "Photothermal Control over the Mechanical and Physical Properties of Polydimethylsiloxane."

1.4 Heterogeneous Catalysis and the Sabatier Reaction

1.4.1 Heterogeneous Catalysis

Heterogeneous catalysis generally occurs in three phases. The first is adsorption of reactants onto the surface of the catalyst; anywhere between one or all the reactants can be adsorbed onto the surface. Then, once the necessary species is on the surface, the reaction can occur (presuming the reacting species are able to meet on the surface), leaving the product adsorbed to the surface. Finally, the product desorbs from the catalyst. In all three of these steps, the affinity of the catalyst for each species is important, as well as the thermodynamic state of the system. The catalyst must hold tightly enough to the reactants that they spend enough time on the surface to react, but not so tightly that the product is stuck to the surface permanently – preventing product formation and inactivating the catalyst. The chemical species, the surface, and nature of the catalyst can all affect this, as well as the pressure and temperature of the system.

Temperature plays a large factor in all these steps, as the thermal motion of the particles is what brings them in contact with the surface, what causes them to move around on the surface, to collide and react with one another, and finally to leave the surface as product species. Increasing temperature will naturally increase the rate of these three phenomena. However, excess temperature can lead to side or reverse reactions as the system equilibrium may shift to favor the reactants or intermediates, reducing conversion.

Heterogeneous catalysis is one of the largest and most important chemical processes currently in use. The most widely used of these processes is the Haber-Bosch conversion of nitrogen and hydrogen gas into ammonia, which can then be used to produce fertilizer. This fertilizer is responsible for feeding a huge portion of the world's population today[50], and the process to synthesize it requires a huge amount of energy in the form of natural gas as well as other energy. Estimates say that nitrogen fertilizer production uses approximately 1% of global primary energy use[51]. Like the Sabatier process, this reaction takes place at very high temperatures (500 °C), but unlike the Sabatier process it also occurs at high pressures (>100 bar) to further increase the reaction rate[52].

1.4.2 Sabatier Reaction

Paul Sabatier was a French chemist from the late 19th century. He helped develop the emerging science of heterogeneous catalysis by identifying that chemical species went through intermediate steps on the surface of a catalyst. This discovery led to further work to develop hydrogenation catalysts, where hydrogen gas is added to organic compounds on a metal surface[53]. He won the Nobel Prize in Chemistry along

---

[50] Erisman et al., "How a Century of Ammonia Synthesis Changed the World."
[51] Worrell et al., "Energy Use and Energy Intensity of the U.S. Chemical Industry."
[52] "Ammonia, 4. Production."

[53] "Paul Sabatier - Biographical."

with Victor Grignard for this work[54]. The most fundamental of these processes, the hydrogenation of carbon dioxide, is named for him. This is the primary reaction of study for this proposal.

$$CO_2 + 4H_2 \leftrightarrow CH_4 + 2H_2O + 165\ \text{kJ}$$

Equation 1: Sabatier reaction.

The addition of hydrogen to CO_2 to form both water and methane is one of several reactions that can occur on a catalytic surface with these species. Based on the chosen catalyst, reaction temperature, and ratio of initial reactants, CO may be the main product. The reaction is also reversible, so methane or CO can be converted back. In **Figure 9** we see that the equilibrium of the system shifts as a function of temperature[55]. However, since reaction rates can be essentially non-existent at low temperatures, a

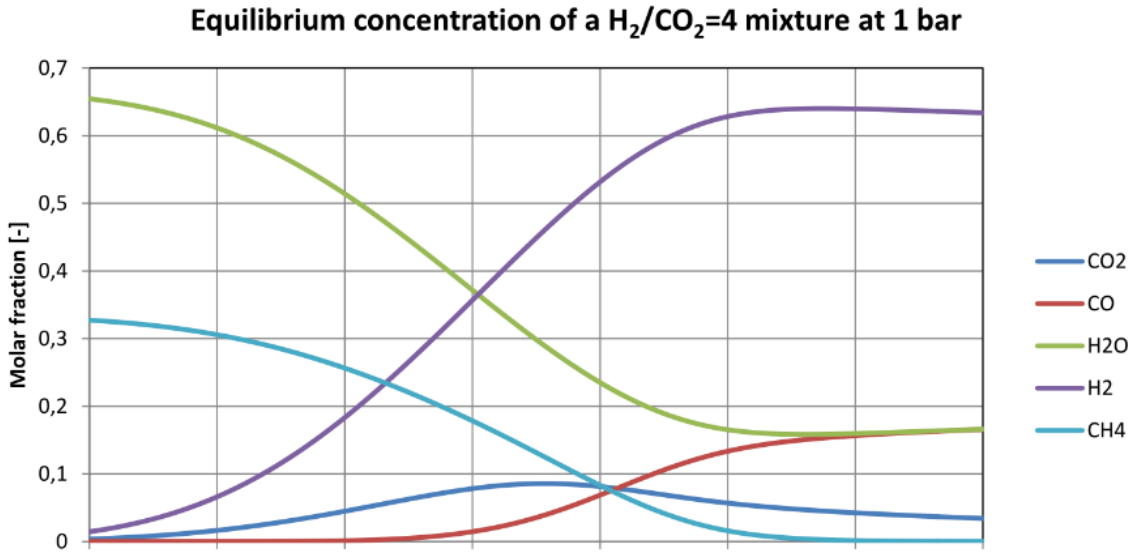

Figure 9: Equilibrium of a stochiometric reaction mixture based on temperature. Courtesy of HELMETH

[54] "The Nobel Prize in Chemistry 1912."
[55] "HELMETH - Methanation Process."

careful balance must be found between both rapid reaction and high conversion. High conversion is important as separation of species is a highly energy-intensive process, therefore the efficiency of any catalytic system is inherently reduced when it is required[56].

Currently the Sabatier process is not used on a large industrial scale. Methane is readily available from natural gas, and the efficiency of the Sabatier process is not yet at the point of competitiveness with simply retrieving such resources from the ground. Similarly, current efficiency limits on this process as well as the production of hydrogen gas limits the industrial feasibility of solar-to-gas plant. The most prominent use of the Sabatier reaction occurs aboard the International Space Station. Installed in 2010, the reactor converts excess hydrogen and carbon dioxide into valuable water, as well as methane which can be further transformed via the Bosch reaction to form elemental carbon and more water[57]. Due to water scarcity aboard the vessel, this reaction is of vital importance to the functioning of a manned spacecraft. Plans for travel to Mars also include water recycling systems, and there is discussion of using the CO_2 rich atmosphere of Mars to generate water via the Sabatier reaction[58].

---

[56] "Materials for Separation Technologies. Energy and Emission Reduction Opportunities."
[57] Junaedi, "Compact and Lightweight Sabatier Reactor for Carbon Dioxide Reduction."
[58] Meier et al., "Mars Atmospheric Conversion to Methane and Water."

The Sabatier reaction is potentially an incredibly important chemical reaction for future energy technology, both on earth and in space. An improved way to perform this reaction with both high efficiency and conversion is therefore desirable.

1.4.3 Photothermal Catalysis

Photothermal catalysis is loosely defined as systems where light heats a system an enables catalysis. In this case we specifically mean nanomaterial-based catalytic systems that have been designed to translate light into heat for catalysis. In many cases the light does a combination of heating and photoelectric enhancement. Our work on the Sabatier reaction is far from the only examination of photothermal catalysis. Over the past decade, significant work has been made on developing photothermal catalysts that function on supports, particularly those that are enhanced by the plasmon activity of the metal nanoparticles used[59]. The applications range from solar fuel generation[60], ammonia synthesis[61], chiral synthesis[62], to scrubbing of volatile organic compounds (VOCs)[63].

---

[59] Tang et al., "Solar Fuel from Photo-Thermal Catalytic Reactions with Spectrum-Selectivity"; Kho et al., "A Review on Photo-Thermal Catalytic Conversion of Carbon Dioxide"; Zhu et al., "Solar-Driven Photothermal Nanostructured Materials Designs and Prerequisites for Evaporation and Catalysis Applications."
[60] Tang et al., "Solar Fuel from Photo-Thermal Catalytic Reactions with Spectrum-Selectivity."
[61] Oshikiri, Ueno, and Misawa, "Plasmon-Induced Ammonia Synthesis through Nitrogen Photofixation with Visible Light Irradiation."
[62] Ma et al., "Photothermal Conversion Triggered Thermal Asymmetric Catalysis within Metal Nanoparticles Loaded Homochiral Covalent Organic Framework."
[63] Jiang et al., "Low-Temperature Photothermal Catalytic Oxidation of Toluene on a Core/Shell SiO2@Pt@ZrO2 Nanostructure."

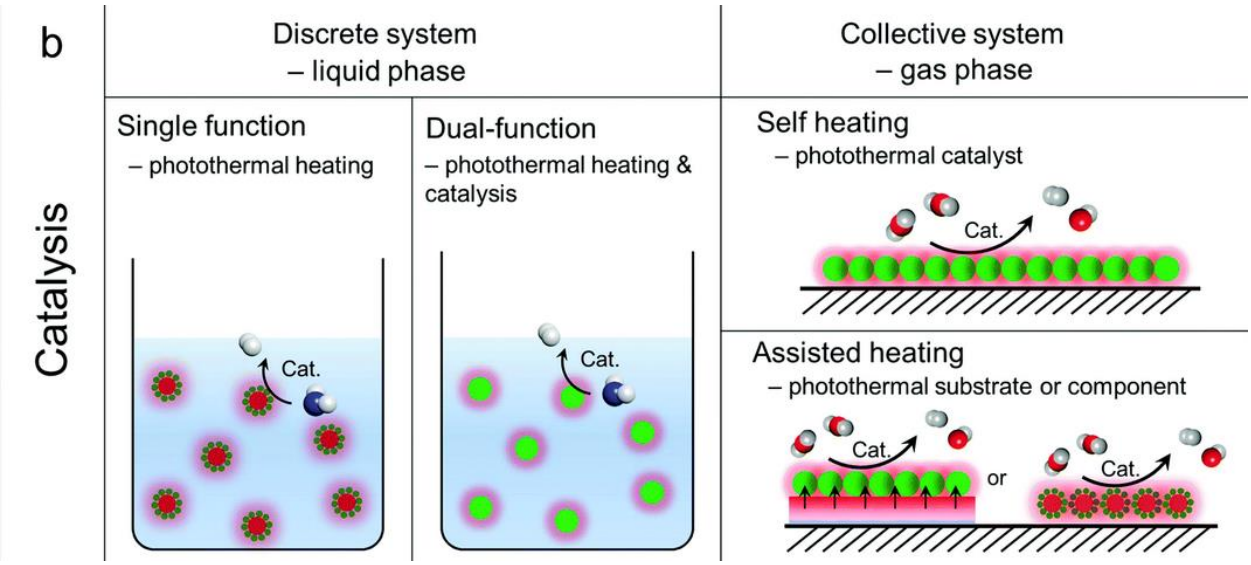

Figure 10: Different approaches to photothermal catalysis, highlighting the dual roles that the nanoparticles can take on in the system.[64]

Our methanation system falls into a different category as compared to most of the ones studied here, as our system is a dual-function system where the particles are dispersed in gas, rather than liquid. The photothermal catalytic systems take advantage of both the localized heating as well as the plasmonic effects that can enhance the reaction of the systems. The benefits of these are very impressive, but often involve complicated material synthesis (metal organic frameworks, composite nanomaterials, etc.) and costly materials. In the chiral synthesis example from Ma et al.[65], the material developed was a covalent organic framework that contained a copper porphyrin as the

[64] Zhu et al., "Solar-Driven Photothermal Nanostructured Materials Designs and Prerequisites for Evaporation and Catalysis Applications."
[65] Ma et al., "Photothermal Conversion Triggered Thermal Asymmetric Catalysis within Metal Nanoparticles Loaded Homochiral Covalent Organic Framework."

photothermal element. The rest of the system, including the framework, worked to perform the asymmetric sterics-driven couplings. This allowed them to do low-temperature, highly selective versions of these reactions at low bulk temperatures (though external heating was still necessary).

In another paper, Jiang et al.[66], showed that a composite nanoparticle could be used to enhance the oxidation of toluene. In this case they took porous silica nanoparticles, doped them with platinum (Pt) nanoparticles, and coated the whole thing with zirconium oxide (ZrO_2). The silica was used as scaffolding, that allowed the Pt nanoparticles and the ZrO_2 to couple electronically. These showed marked improvement in their catalytic activity when they were illuminated as well as heated, instead of just being heated. The mechanism for this reaction requires steps that are just thermal, as well as steps mediated by the photocatalytic activity of the ZrO_2, as the photothermal heating of the Pt nanoparticles assists with both, it helps the system perform complete oxidation of the VOCs rapidly.

Of course, it is worth discussing the competing literature to our project, that is, other photothermal catalysts for methanation of carbon dioxide. There are numerous

[66] Jiang et al., "Low-Temperature Photothermal Catalytic Oxidation of Toluene on a Core/Shell SiO2@Pt@ZrO2 Nanostructure."

examples in the literature[67], as well as several recent reviews[68]. These systems are developed using classical catalytic pairs of catalyst and support, sometimes with the photothermal element being decoupled from the catalyst. There have been high-yield, low temperature, and high selectivity results, although almost all require external heating, and all involve relatively complex nanoengineering. The advantage our project has is that we've looked at utilizing exclusively Nickel, which is cheap, abundant, and requires very little in the way of treatment or handling to remain a robust and selective catalyst for methanation.

1.4.4 Catalysis for Methanation

Currently, commercial methanation almost always occurs on nickel catalysts, as it is both affordable and highly selective[69]. Catalysis is done thermally, on metal-oxide supports to increase the surface area[55]. While significant research is being done to explore low temperature methanation for industrial use (low temperature being around 200 °C), the lack of systems that allow for scale-up or temperatures below 200 °C has

---

[67] Jantarang et al., "Role of Support in Photothermal Carbon Dioxide Hydrogenation Catalysed by Ni/CexTiyO2"; Kho et al., "Harnessing the Beneficial Attributes of Ceria and Titania in a Mixed-Oxide Support for Nickel-Catalyzed Photothermal CO2 Methanation"; Li et al., "Selective Light Absorber-Assisted Single Nickel Atom Catalysts for Ambient Sunlight-Driven CO 2 Methanation"; Meng et al., "Photothermal Conversion of CO_2 into CH_4 with H_2 over Group VIII Nanocatalysts"; Kim et al., "Energy-Efficient CO 2 Hydrogenation with Fast Response Using Photoexcitation of CO 2 Adsorbed on Metal Catalysts"; Zhou et al., "Light-Driven Methane Dry Reforming with Single Atomic Site Antenna-Reactor Plasmonic Photocatalysts."

[68] Ghoussoub et al., "Principles of Photothermal Gas-Phase Heterogeneous CO2 Catalysis"; Kho et al., "A Review on Photo-Thermal Catalytic Conversion of Carbon Dioxide."

[69] Rönsch et al., "Review on Methanation – From Fundamentals to Current Projects."

been identified as an issue in the wider implementation of methanation technology[70]. While advances in supports and promotors have been advancing the field, supported nickel under high pressure and high temperature is still the industry standard[55].

As referenced in the previous section, there has been both photocatalysis and photothermal catalysis for methanation. The photothermal catalysis is most relevant and reviewed more thoroughly in the previous, but the photocatalytic systems currently being studied are photoredox system, where absorbed light on a catalyst is used to directly reduce the reactants, often in multiple steps[71]. Often these materials are meant to be combined with similar photocatalytic systems for water splitting. A few of these systems have produced impressive results under optimized settings, producing hydrogen and methane from CO_2 and water under ambient temperature and pressure. The lack of stability, precise wavelength needed, and low quantum yield prevent this from being the technology it needs to be to replace other forms of methanation, but it is still a promising area of research.

There is also biocatalysis, where microbes that absorb either light, heat or both do the catalytic conversion. These engineered microbes are bioengineered to take light,

[70] Lee et al., "Recent Trend in Thermal Catalytic Low Temperature CO2 Methanation."
[71] Ulmer et al., "Fundamentals and Applications of Photocatalytic CO 2 Methanation."

heat and CO_2 and convert it to methane[72]. There are some impressive pilot plants utilizing this technology in the EU, and it continues to be a promising area.

1.5 Finite Element Analysis

Finite Element Analysis (FEM) was a key tool in several of my projects, all utilizing the software suite COMSOL. FEM is a numerical way to solve partial differential equations by dividing up the space and time of the system into discrete elements. Many engineering and physics problems can be modeled this way, and we've used it to examine spatial reactor designs. COMSOL is a software that lets you work through the problem visually and define which methods of solving which PDEs in each system[73].

1.5.1 Partial Differential Equations

In the Ascaridole reactor project, we utilize the canon of any chemical engineer; chemical transport, liquid motion, and heat conduction. In the acoustic polymerization project, we complete the team with an exploration of stress and strain on an oscillating system.

---

[72] Ulmer et al.
[73] "COMSOL Multiphysics Reference Manual, Version 5.3."

The equations that define all these different elements of physics are interrelated and can grow infinitely complex the more detail we dive into. (It's theoretically possible to model something starting at the quark scale, but only if you have a couple billion universe lifetimes to spare). We therefore choose to keep our finite division of the problem space and time limited, as well as make some assumptions about how the system works based on the materials and physical scales we're working with.

1.5.1.1 Chemical Transport

From a chemistry perspective, it's common to examine chemical reactions in the zeroth dimension, assuming everything is well mixed, and the only important factors are the quantities and the time. However, when trying out new spatial chemistry or reactor designs it's important to keep diffusion and fluid transport in mind when you're working on optimizing any sort of process.

Using FEM to predict these results means using the Navier-Stokes Equation for the fluid motion, diffusion problems for all the chemical species and the rate of their reactions at any given point, plus thermal transport for the whole system, usually complicated by heats of reaction. All these equations are impossible to solve analytically, which makes FEM the best option to solve it numerically.

COMSOL is very helpful with all this, but it does require all the qualities of the fluid as well as the versions of the equations you're using, meaning both assumptions

and measurements about and of the system are necessary, and the model accuracy depends on doing this properly and thoughtfully. In our microfluidic system it was simple to look at similar microfluidic systems and check how they decided on their assumptions, but if it hadn't been a dilute methanol solution that may not have been the right call.

1.5.1.2 Mechanical Stress

Very similar to the above problem, but instead of the equations for diffusion and flow, you're looking at the relationships between force, stress, and strain in the material. Stress is a measure of the force being exerted on the material by itself, or rather if you look at a single point in the material, the forces exerted on that point by the surrounding material. Strain is the deformation of the material, which of course can be wildly different based on the material (gum vs steel vs wood). The finite element method was originally developed to help provide numerical solutions to the partial differential equations that describe stress-strain relationships.

The material we were performing calculations on is a gel that began in a very elastic state and stiffened in response to repeated stress. This means that in its initial state it will respond to even small forces by deforming; but since the material stiffens, with repeated loadings of force, the material will deform less and less over time.

The equations solved are borne out of a formation of Newton's second law. We chose to use conditions suitable for an elastic material because all the modeling of the material was in its malleable, pre-stiffened state.

1.6 Acoustic Polymerization with Nanoparticles for Adaptive Materials

The system that I model in chapter 4 b is based on one of the Esser-Kahn Lab's many piezoelectric nanoparticle-based dynamic reaction systems. In **Figure 11**, is a diagram showing a different example of these systems. The core concept is that piezoelectric nanoparticles respond to stress by creating a dipole, and this dipole, through a yet to be determined process, reduces a metal ion, which then goes on to participate in a reaction that alters the material. In this earlier paper, the copper click reaction was used to perform an atom-transfer radical polymerization (ATRP) reaction, which was able to generate a very particular size of polymer by adjusting the time of sonication.

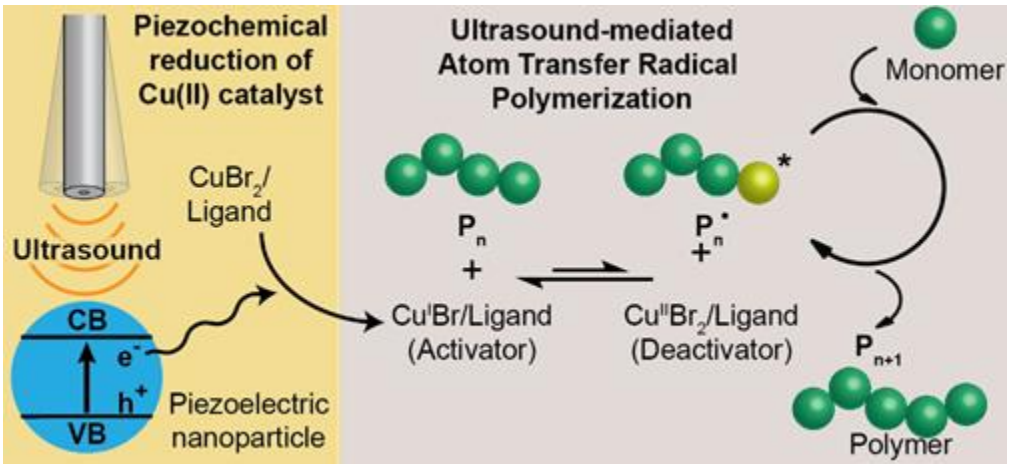

Figure 11: Image depicting acoustic polymerization from Mohapatra et al.[74]

The system modeled in chapter 4 however, represents several years advancement beyond the above project. Now rather than in solution with ultrasound, this reaction occurs within an already made organo-gel and creates a secondary structure to stiffen and strengthen the gel in response to stress. Then this system can be further stressed to crosslink this internal network.

In this case, the reaction system uses a different type of piezoelectric nanoparticle (zinc oxide), as well as a different reaction system. This system is swelled into the gel, where it can be used to build this secondary internal network.

[74] Mohapatra, Kleiman, and Esser-Kahn, "Mechanically Controlled Radical Polymerization Initiated by Ultrasound."

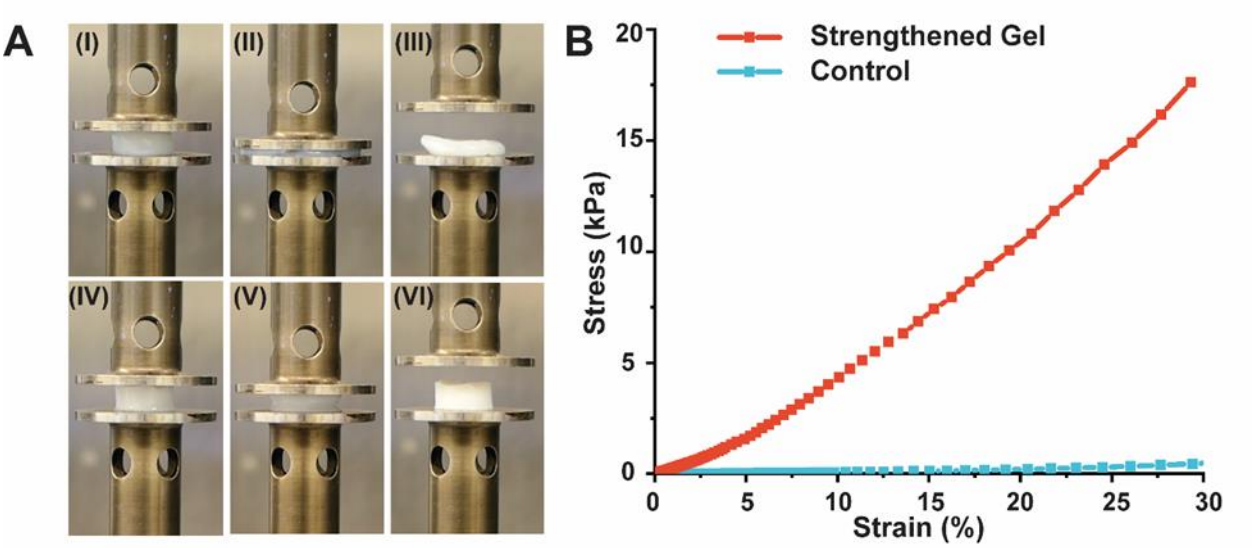

Figure 12: Preprint publication on novel material stress-strain relationship between strengthened and unstrengthened material.

The result is a material that can be strengthened through repeated stress, in this case by sonic scale vibrations. But it is the stress within the material that causes this, as the nanoparticles still need to be stressed by the surrounding gel network. Since depending on the material, stress may not be applied evenly, so I was enlisted to perform the computational exploration of how a gel like this might respond to oscillations.

1.7 Ascaridole Production

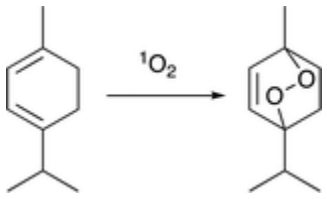

Figure 13: Conversion of α-terpinene to ascaridole using singlet oxygen

Ascaridole is a natural product of wormseed and is used as an antiparasitic in both Western and traditional medicine[75]. We're modeling the conversion of α-terpinene into it by the addition of singlet oxygen. This is a simple reduction of the conjugated alkenes in the ring of α-terpinene. Singlet oxygen is being generated at a constant rate throughout the microfluidic system as the reaction system flows through.

1.8 Photon Upconversion

Photon upconversion is essentially a molecular system where light is captured, combined, and then rereleased at a lower wavelength. These systems have two elements that need to be conjugated together. A photon "catcher" that accepts and stabilizes the energy from the photons, and then the emitter that gathers the energy from multiple lower energy photons and emits them as a high energy one of a specific wavelength[76].

[75] Dembitsky, Shkrob, and Hanus, "ASCARIDOLE AND RELATED PEROXIDES FROM THE GENUS CHENOPODIUM."
[76] Kim et al., "High Efficiency Low-Power Upconverting Soft Materials."

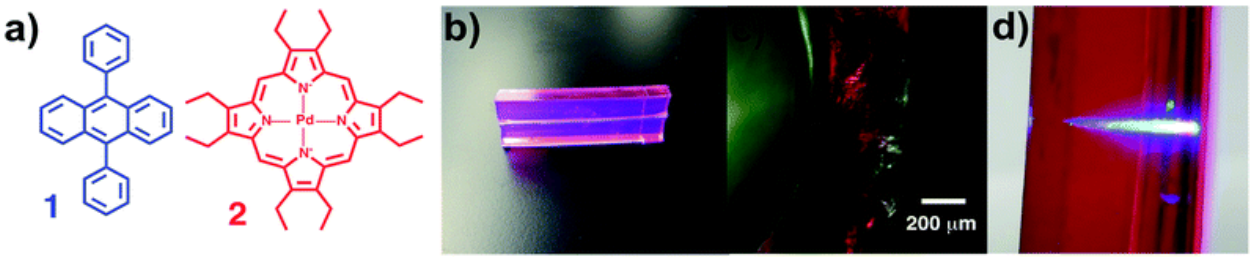

Figure 14: Figure showing a) upconversion pair, and b) & d) the upconversion occurring in the polyurethane[77]

In the microfluidic system discussed in chapter 4b, the upconversion materials were embedded in a polyurethane system that the microfluid reaction system ran through[78]. This converted the nonspecific solar spectrum light into higher energy blue light that could be absorbed to produce singlet oxygen within the fluid mixture.

[77] Wu et al., "Photon Upconversion for the Enhancement of Microfluidic Photochemical Synthesis."
[78] Simon and Weder, "Low-Power Photon Upconversion through Triplet–Triplet Annihilation in Polymers."

Introduction Bibliography

A. Herron, Jeffrey, Jiyong Kim, Aniruddha A. Upadhye, George W. Huber, and Christos T. Maravelias. "A General Framework for the Assessment of Solar Fuel Technologies." *Energy & Environmental Science* 8, no. 1 (2015): 126–57. https://doi.org/10.1039/C4EE01958J.

Alabastri, Alessandro, Pratiksha D. Dongare, Oara Neumann, Jordin Metz, Ifeoluwa Adebiyi, Peter Nordlander, and Naomi J. Halas. "Resonant Energy Transfer Enhances Solar Thermal Desalination." *Energy & Environmental Science* 13, no. 3 (March 18, 2020): 968–76. https://doi.org/10.1039/C9EE03256H.

"Ammonia, 4. Production." In *Ullmann's Encyclopedia of Industrial Chemistry*. Wiley-VCH Verlag GmbH & Co. KGaA, 2006.

Ayala-Orozco, Ciceron, Cordula Urban, Sandra Bishnoi, Alexander Urban, Heather Charron, Tamika Mitchell, Martin Shea, et al. "Sub-100nm Gold Nanomatryoshkas Improve Photo-Thermal Therapy Efficacy in Large and Highly Aggressive Triple Negative Breast Tumors." *Journal of Controlled Release*, Eleventh International Nanomedicine and Drug Delivery Symposium, 191 (October 10, 2014): 90–97. https://doi.org/10.1016/j.jconrel.2014.07.038.

Barnett, Benjamin, and William E. Vaughan. "The Decomposition of Benzoyl Peroxide. I. The Kinetics and Stoichiometry in Benzene." *The Journal of Physical and Colloid Chemistry* 51, no. 4 (April 1, 1947): 926–42. https://doi.org/10.1021/j150454a003.

Brinson, Bruce E., J. Britt Lassiter, Carly S. Levin, Rizia Bardhan, Nikolay Mirin, and Naomi J. Halas. "Nanoshells Made Easy: Improving Au Layer Growth on Nanoparticle Surfaces." *Langmuir* 24, no. 24 (December 16, 2008): 14166–71. https://doi.org/10.1021/la802049p.

Brongersma, Mark L., Naomi J. Halas, and Peter Nordlander. "Plasmon-Induced Hot Carrier Science and Technology." *Nature Nanotechnology* 10, no. 1 (January 2015): 25–34. https://doi.org/10.1038/nnano.2014.311.

Cain, John R. "Lunar Dust: The Hazard and Astronaut Exposure Risks." *Earth, Moon, and Planets* 107, no. 1 (December 1, 2010): 107–25. https://doi.org/10.1007/s11038-010-9365-0.

Chen, Jianing, Pablo Albella, Zhaleh Pirzadeh, Pablo Alonso-González, Florian Huth, Stefano Bonetti, Valentina Bonanni, et al. "Plasmonic Nickel Nanoantennas." *Small* 7, no. 16 (August 22, 2011): 2341–47. https://doi.org/10.1002/smll.201100640.

Chen, Wenxue, Ciceron Ayala-Orozco, Nrusingh C. Biswal, Carlos Perez-Torres, Marc Bartels, Rizia Bardhan, Gary Stinnet, et al. "Targeting of Pancreatic Cancer with Magneto-Fluorescent Theranostic Gold Nanoshells." *Nanomedicine (London, England)* 9, no. 8 (June 2014): 1209–22. https://doi.org/10.2217/nnm.13.84.

Chris Toumey. "Apostolic Succession." *Engineering & Science* 1 (2005): 16–23.

Co, Aldrich Chenical. "Free Radical Initiators," n.d., 2.

Cole, Joseph R., Nikolay A. Mirin, Mark W. Knight, Glenn P. Goodrich, and Naomi J. Halas. "Photothermal Efficiencies of Nanoshells and Nanorods for Clinical Therapeutic Applications." *The Journal of Physical Chemistry C* 113, no. 28 (July 16, 2009): 12090–94. https://doi.org/10.1021/jp9003592.

"COMSOL Multiphysics Reference Manual, Version 5.3." Comsol, Inc, n.d. http://www.comsol.com/.

Dembitsky, Valery, Ilya Shkrob, and Lumir Ondrej Hanus. "ASCARIDOLE AND RELATED PEROXIDES FROM THE GENUS CHENOPODIUM." *Biomedical Papers* 152, no. 2 (December 1, 2008): 209–15. https://doi.org/10.5507/bp.2008.032.

Donnet, Jean-Baptiste, and Andries Voet. *Carbon Black: Physics, Chemistry, and Elastomer Reinforcement*. New York: M. Dekker, 1976.

Dutcher, Bryce, Maohong Fan, and Armistead G. Russell. "Amine-Based CO2 Capture Technology Development from the Beginning of 2013—A Review." *ACS Applied Materials & Interfaces* 7, no. 4 (February 4, 2015): 2137–48. https://doi.org/10.1021/am507465f.

Erisman, Jan Willem, Mark A. Sutton, James Galloway, Zbigniew Klimont, and Wilfried Winiwarter. "How a Century of Ammonia Synthesis Changed the World." Special Features. Nature Geoscience, September 28, 2008. https://doi.org/10.1038/ngeo325.

Feynman, Richard P. "Plenty of Room at the Bottom," n.d., 7.

Fortenbaugh, R. Joseph, Sabrina A. Carrozzi, and Benjamin J. Lear. "Photothermal Control over the Mechanical and Physical Properties of Polydimethylsiloxane." *Macromolecules* 52, no. 10 (May 28, 2019): 3839–44. https://doi.org/10.1021/acs.macromol.9b00134.

Fortenbaugh, R. Joseph, and Benjamin J. Lear. "On-Demand Curing of Polydimethylsiloxane (PDMS) Using the Photothermal Effect of Gold Nanoparticles." *Nanoscale* 9, no. 25 (June 29, 2017): 8555–59. https://doi.org/10.1039/C7NR01423F.

Gao, Minmin, Liangliang Zhu, Connor Kangnuo Peh, and Ghim Wei Ho. "Solar Absorber Material and System Designs for Photothermal Water Vaporization towards Clean Water and Energy Production." *Energy & Environmental Science* 12, no. 3 (March 13, 2019): 841–64. https://doi.org/10.1039/C8EE01146J.

Ghoussoub, Mireille, Meikun Xia, Paul N. Duchesne, Dvira Segal, and Geoffrey Ozin. "Principles of Photothermal Gas-Phase Heterogeneous CO2 Catalysis." *Energy & Environmental Science* 12, no. 4 (April 10, 2019): 1122–42. https://doi.org/10.1039/C8EE02790K.

Haas, Kaitlin M., and Benjamin J. Lear. "Billion-Fold Rate Enhancement of Urethane Polymerization via the Photothermal Effect of Plasmonic Gold Nanoparticles." *Chemical Science* 6, no. 11 (October 13, 2015): 6462–67. https://doi.org/10.1039/C5SC02149A.

Han, Dongxiao, Zhaoguo Meng, Daxiong Wu, Canying Zhang, and Haitao Zhu. "Thermal Properties of Carbon Black Aqueous Nanofluids for Solar Absorption." *Nanoscale Research Letters* 6, no. 1 (July 18, 2011): 457. https://doi.org/10.1186/1556-276X-6-457.

"HELMETH - Methanation Process." Accessed February 1, 2018. http://helmeth.eu/index.php/technologies/methanation-process.

Hirsch, L.R., R.J. Stafford, J.A. Bankson, S.R. Sershen, R.E. Price, J.D. Hazle, N.J. Halas, and J.L. West. "Targeted Photothermal Tumor Therapy Using Metal Nanoshells." In *Proceedings of the Second Joint 24th Annual Conference and the Annual Fall Meeting of the Biomedical Engineering Society] [Engineering in Medicine and Biology*, 1:530–31 vol.1, 2002. https://doi.org/10.1109/IEMBS.2002.1136933.

Hogan, Nathaniel J., Alexander S. Urban, Ciceron Ayala-Orozco, Alberto Pimpinelli, Peter Nordlander, and Naomi J. Halas. "Nanoparticles Heat through Light Localization." *Nano Letters* 14, no. 8 (August 13, 2014): 4640–45. https://doi.org/10.1021/nl5016975.

Jantarang, Salina, Emma C. Lovell, Tze Hao Tan, Jason Scott, and Rose Amal. "Role of Support in Photothermal Carbon Dioxide Hydrogenation Catalysed by Ni/CexTiyO2." *Progress in Natural Science: Materials International* 28, no. 2 (April 1, 2018): 168–77. https://doi.org/10.1016/j.pnsc.2018.02.004.

Jiang, Chunli, Hao Wang, Shengzhi Lin, Fei Ma, Yongqing Wang, and Hongbing Ji. "Low-Temperature Photothermal Catalytic Oxidation of Toluene on a Core/Shell SiO2@Pt@ZrO2 Nanostructure." *Industrial & Engineering Chemistry Research* 58, no. 36 (September 11, 2019): 16450–58. https://doi.org/10.1021/acs.iecr.9b02850.

Jones, Steven, Daniel Andrén, Tomasz J. Antosiewicz, and Mikael Käll. "Ultrafast Modulation of Thermoplasmonic Nanobubbles in Water." *Nano Letters* 19, no. 11 (November 13, 2019): 8294–8302. https://doi.org/10.1021/acs.nanolett.9b03895.

Junaedi, ChristianHawley. "Compact and Lightweight Sabatier Reactor for Carbon Dioxide Reduction." Portland, OR, United States, 2011. https://ntrs.nasa.gov/search.jsp?R=20120016419.

Kaur, Manmeet, and A. K. Srivastava. "Photopolymerization: A Review." *Journal of Macromolecular Science, Part C* 42, no. 4 (January 12, 2002): 481–512. https://doi.org/10.1081/MC-120015988.

Khlebtsov, Nikolai G., and Lev A. Dykman. "Optical Properties and Biomedical Applications of Plasmonic Nanoparticles." *Journal of Quantitative Spectroscopy and Radiative Transfer* 111, no. 1 (January 1, 2010): 1–35. https://doi.org/10.1016/j.jqsrt.2009.07.012.

Kho, Ee Teng, Salina Jantarang, Zhaoke Zheng, Jason Scott, and Rose Amal. "Harnessing the Beneficial Attributes of Ceria and Titania in a Mixed-Oxide Support for Nickel-Catalyzed Photothermal CO2 Methanation." *Engineering* 3, no. 3 (June 1, 2017): 393–401. https://doi.org/10.1016/J.ENG.2017.03.016.

Kho, Ee Teng, Tze Hao Tan, Emma Lovell, Roong Jien Wong, Jason Scott, and Rose Amal. "A Review on Photo-Thermal Catalytic Conversion of Carbon Dioxide." *Green Energy & Environment*, Special Issue on Energy Storage and Conversion, 2, no. 3 (July 1, 2017): 204–17. https://doi.org/10.1016/j.gee.2017.06.003.

Kim, Chanyeon, Seokwon Hyeon, Jonghyeok Lee, Whi Dong Kim, Doh C. Lee, Jihan Kim, and Hyunjoo Lee. "Energy-Efficient CO 2 Hydrogenation with Fast Response Using Photoexcitation of CO 2 Adsorbed on Metal Catalysts." *Nature Communications* 9, no. 1 (August 2, 2018): 3027. https://doi.org/10.1038/s41467-018-05542-5.

Kim, Jae-Hyuk, Fan Deng, Felix N. Castellano, and Jae-Hong Kim. "High Efficiency Low-Power Upconverting Soft Materials." *Chemistry of Materials* 24, no. 12 (June 26, 2012): 2250–52. https://doi.org/10.1021/cm3012414.

Lal, Surbhi, Susan E. Clare, and Naomi J. Halas. "Nanoshell-Enabled Photothermal Cancer Therapy: Impending Clinical Impact." *Accounts of Chemical Research* 41, no. 12 (December 16, 2008): 1842–51. https://doi.org/10.1021/ar800150g.

Lee, Woo Jin, Chaoen Li, Hermawan Prajitno, Jiho Yoo, Jim Patel, Yunxia Yang, and Seng Lim. "Recent Trend in Thermal Catalytic Low Temperature CO2 Methanation: A Critical Review." *Catalysis Today*, February 20, 2020. https://doi.org/10.1016/j.cattod.2020.02.017.

Leung, Dennis Y. C., Giorgio Caramanna, and M. Mercedes Maroto-Valer. "An Overview of Current Status of Carbon Dioxide Capture and Storage Technologies." *Renewable and Sustainable Energy Reviews* 39 (November 1, 2014): 426–43. https://doi.org/10.1016/j.rser.2014.07.093.

Li, Jing-Liang, and Min Gu. "Gold-Nanoparticle-Enhanced Cancer Photothermal Therapy." *IEEE Journal of Selected Topics in Quantum Electronics* 16, no. 4 (July 2010): 989–96. https://doi.org/10.1109/JSTQE.2009.2030340.

Li, Yaguang, Jianchao Hao, Hui Song, Fengyu Zhang, Xianhua Bai, Xianguang Meng, Hongyuan Zhang, Shufang Wang, Yong Hu, and Jinhua Ye. "Selective Light Absorber-Assisted Single Nickel Atom Catalysts for Ambient Sunlight-Driven CO 2 Methanation." *Nature Communications* 10, no. 1 (May 29, 2019): 2359. https://doi.org/10.1038/s41467-019-10304-y.

Ma, Hui-Chao, Chen-Chen Zhao, Gong-Jun Chen, and Yu-Bin Dong. "Photothermal Conversion Triggered Thermal Asymmetric Catalysis within Metal Nanoparticles Loaded Homochiral Covalent Organic Framework." *Nature Communications* 10, no. 1 (July 29, 2019): 3368. https://doi.org/10.1038/s41467-019-11355-x.

Mann, Michael E., and Lee R. Kump. *Dire Predictions: Understanding Climate Change*. Second American edition. New York, NY: DK, 2015.

"Materials for Separation Technologies. Energy and Emission Reduction Opportunities." Oak Ridge National Lab. (ORNL), Oak Ridge, TN (United States), May 4, 2005. https://doi.org/10.2172/1218755.

Meier, Anne, Malay Shah, Paul Hintze, Elspeth Petersen, and Anthony Muscatello. "Mars Atmospheric Conversion to Methane and Water: An Engineering Model of the Sabatier Reactor with Characterization of Ru/Al2O3 for Long Duration Use on Mars," July 16, 2017. https://ttu-ir.tdl.org/ttu-ir/handle/2346/72974.

Meng, Xianguang, Tao Wang, Lequan Liu, Shuxin Ouyang, Peng Li, Huilin Hu, Tetsuya Kako, Hideo Iwai, Akihiro Tanaka, and Jinhua Ye. "Photothermal Conversion of CO_2 into CH_4 with H_2 over Group VIII Nanocatalysts: An Alternative Approach for Solar Fuel Production." *Angewandte Chemie (International Ed. in English)* 53, no. 43 (October 20, 2014): 11478–82. https://doi.org/10.1002/anie.201404953.

Mohapatra, Hemakesh, Maya Kleiman, and Aaron Palmer Esser-Kahn. "Mechanically Controlled Radical Polymerization Initiated by Ultrasound." *Nature Chemistry* 9, no. 2 (February 2017): 135–39. https://doi.org/10.1038/nchem.2633.

Neumann, Oara, Curtis Feronti, Albert D. Neumann, Anjie Dong, Kevin Schell, Benjamin Lu, Eric Kim, et al. "Compact Solar Autoclave Based on Steam Generation Using Broadband Light-Harvesting Nanoparticles." *Proceedings of the National Academy of Sciences* 110, no. 29 (July 16, 2013): 11677–81. https://doi.org/10.1073/pnas.1310131110.

Neumann, Oara, Albert D. Neumann, Shu Tian, Christyn Thibodeaux, Shobhit Shubhankar, Julius Müller, Edgar Silva, et al. "Combining Solar Steam Processing and Solar Distillation for Fully Off-Grid Production of Cellulosic Bioethanol." *ACS Energy Letters* 2, no. 1 (January 13, 2017): 8–13. https://doi.org/10.1021/acsenergylett.6b00520.

Neumann, Oara, Alexander S. Urban, Jared Day, Surbhi Lal, Peter Nordlander, and Naomi J. Halas. "Solar Vapor Generation Enabled by Nanoparticles." *ACS Nano* 7, no. 1 (January 22, 2013): 42–49. https://doi.org/10.1021/nn304948h.

Nguyen, Du T., Richard Truong, Richard Lee, Samantha A. Goetz, and Aaron P. Esser-Kahn. "Photothermal Release of CO2 from Capture Solutions Using Nanoparticles." *Energy & Environmental Science* 7, no. 8 (July 18, 2014): 2603–7. https://doi.org/10.1039/C4EE01047G.

Odian, George G. *Principles of Polymerization*. 4th ed. Hoboken, N.J: Wiley-Interscience, 2004.

Oshikiri, Tomoya, Kosei Ueno, and Hiroaki Misawa. "Plasmon-Induced Ammonia Synthesis through Nitrogen Photofixation with Visible Light Irradiation." *Angewandte Chemie International Edition* 53, no. 37 (September 8, 2014): 9802–5. https://doi.org/10.1002/anie.201404748.

"Paul Sabatier - Biographical." Accessed February 1, 2018. https://www.nobelprize.org/nobel_prizes/chemistry/laureates/1912/sabatier-bio.html.

Raj K. Keservani, and Anil K. Sharma. *Nanoparticulate Drug Delivery Systems*. CRC Press, 2019.

Richardson, Hugh H., Zackary N. Hickman, Alexander O. Govorov, Alyssa C. Thomas, Wei Zhang, and Martin E. Kordesch. "Thermooptical Properties of Gold Nanoparticles Embedded in Ice: Characterization of Heat Generation and Melting." *Nano Letters* 6, no. 4 (April 1, 2006): 783–88. https://doi.org/10.1021/nl060105l.

Robatjazi, Hossein, Hangqi Zhao, Dayne F. Swearer, Nathaniel J. Hogan, Linan Zhou, Alessandro Alabastri, Michael J. McClain, Peter Nordlander, and Naomi J. Halas. "Plasmon-Induced Selective Carbon Dioxide Conversion on Earth-Abundant Aluminum-Cuprous Oxide Antenna-Reactor Nanoparticles." *Nature Communications* 8, no. 1 (June 21, 2017): 27. https://doi.org/10.1038/s41467-017-00055-z.

Roberts, Adam T., Jian Yang, Matthew E. Reish, Alessandro Alabastri, Naomi J. Halas, Peter Nordlander, and Henry O. Everitt. "Plasmonic Nanoparticle-Based Epoxy Photocuring: A Deeper Look." *Materials Today* 27 (July 1, 2019): 14–20. https://doi.org/10.1016/j.mattod.2018.09.005.

Rönsch, Stefan, Jens Schneider, Steffi Matthischke, Michael Schlüter, Manuel Götz, Jonathan Lefebvre, Praseeth Prabhakaran, and Siegfried Bajohr. "Review on Methanation – From Fundamentals to Current Projects." *Fuel* 166 (February 15, 2016): 276–96. https://doi.org/10.1016/j.fuel.2015.10.111.

Scott Dial. "Selected Energy Densities Plot," n.d. https://commons.wikimedia.org/w/index.php?curid=5551431.

Sershen, S.R., N.J. Halas, and J.L. West. "Pulsatile Release of Insulin via Photothermally Modulated Drug Delivery." In *Proceedings of the Second Joint 24th Annual Conference and the Annual Fall Meeting of the Biomedical Engineering Society] [Engineering in Medicine and Biology*, 1:490–91 vol.1, 2002. https://doi.org/10.1109/IEMBS.2002.1136910.

Simon, Yoan C., and Christoph Weder. "Low-Power Photon Upconversion through Triplet–Triplet Annihilation in Polymers." *Journal of Materials Chemistry* 22, no. 39 (September 18, 2012): 20817–30. https://doi.org/10.1039/C2JM33654E.

Swearer, Dayne F., Hossein Robatjazi, John Mark P. Martirez, Ming Zhang, Linan Zhou, Emily A. Carter, Peter Nordlander, and Naomi J. Halas. "Plasmonic Photocatalysis of Nitrous Oxide into N2 and O2 Using Aluminum–Iridium Antenna–Reactor Nanoparticles." *ACS Nano* 13, no. 7 (July 23, 2019): 8076–86. https://doi.org/10.1021/acsnano.9b02924.

Tang, Sanli, Jie Sun, Hui Hong, and Qibin Liu. "Solar Fuel from Photo-Thermal Catalytic Reactions with Spectrum-Selectivity: A Review." *Frontiers in Energy* 11, no. 4 (December 1, 2017): 437–51. https://doi.org/10.1007/s11708-017-0509-z.

"The Nobel Prize in Chemistry 1912." Accessed February 1, 2018. https://www.nobelprize.org/nobel_prizes/chemistry/laureates/1912/.

"Thermal Initiators: Decomposition Rate and Half-Life." Aldrich. Accessed September 6, 2017. http://www.sigmaaldrich.com/content/dam/sigma-aldrich/docs/Aldrich/General_Information/thermal_initiators.pdf.

Ulmer, Ulrich, Thomas Dingle, Paul N. Duchesne, Robert H. Morris, Alexandra Tavasoli, Thomas Wood, and Geoffrey A. Ozin. "Fundamentals and Applications of Photocatalytic CO 2 Methanation." *Nature Communications* 10, no. 1 (July 18, 2019): 3169. https://doi.org/10.1038/s41467-019-10996-2.

Worrell, Ernst, Dian Phylipsen, Dan Einstein, and Nathan Martin. "Energy Use and Energy Intensity of the U.S. Chemical Industry," April 1, 2000. https://escholarship.org/uc/item/2925w8g6.

Wu, M., B. A. Moser, T. M. Steeves, A. Figueroa, B. M. Wallace, S. T. Kim, A. P. Esser-Kahn, and R. C. Steinhardt. "Photon Upconversion for the Enhancement of Microfluidic Photochemical Synthesis." *RSC Advances* 9, no. 45 (2019): 26172–75. https://doi.org/10.1039/C9RA03468D.

Zhou, Linan, John Mark P. Martirez, Jordan Finzel, Chao Zhang, Dayne F. Swearer, Shu Tian, Hossein Robatjazi, et al. "Light-Driven Methane Dry Reforming with Single Atomic Site Antenna-Reactor Plasmonic Photocatalysts." *Nature Energy* 5, no. 1 (January 2020): 61–70. https://doi.org/10.1038/s41560-019-0517-9.

Zhou, Linan, Dayne F. Swearer, Chao Zhang, Hossein Robatjazi, Hangqi Zhao, Luke Henderson, Liangliang Dong, et al. "Quantifying Hot Carrier and Thermal Contributions in Plasmonic Photocatalysis." *Science* 362, no. 6410 (October 5, 2018): 69–72. https://doi.org/10.1126/science.aat6967.

Zhu, Liangliang, Minmin Gao, Connor Kang Nuo Peh, and Ghim Wei Ho. "Solar-Driven Photothermal Nanostructured Materials Designs and Prerequisites for Evaporation and Catalysis Applications." *Materials Horizons* 5, no. 3 (May 8, 2018): 323–43. https://doi.org/10.1039/C7MH01064H.

Photothermal Heating of Carbon Black Nanoparticles for Radical Polymerization

2.1 Bulk Radical Polymerization Initiated by Benzoyl Peroxide

2.1.1 Introduction

As outlined in the background, there has already been several significant publications on utilizing photothermal heating of metallic nanoparticles for dynamic polymerization, degradation, and crosslinking[79]. At the time of publication, the work presented was the only demonstration of initial solution-based polymerization driven solely by photothermal heating. The utility of our version was what it allowed carbon black to serve the dual role of heaters within the solution as well as a common filler to strengthen the polymer. Since the publication of this work, there have been several examples of publications further exploring this concept.

As a disclaimer, much of this chapter has been reworked, adapted, or reproduced from my master's thesis as well as the original publication.

---

[79] Haas and Lear, "Billion-Fold Rate Enhancement of Urethane Polymerization via the Photothermal Effect of Plasmonic Gold Nanoparticles"; Fortenbaugh and Lear, "On-Demand Curing of Polydimethylsiloxane (PDMS) Using the Photothermal Effect of Gold Nanoparticles"; Fortenbaugh, Carrozzi, and Lear, "Photothermal Control over the Mechanical and Physical Properties of Polydimethylsiloxane"; Firestone et al., "Photothermally-Driven Thermo-Oxidative Degradation of Low Density Polyethylene"; Huang et al., "Nanoparticle-Based Photothermal Heating to Drive Chemical Reactions within a Solid."

The photothermal heating of nanoparticles in solution provides a model system to study the spatial control over reaction systems. Previous work in the Esser-Kahn laboratory demonstrated that nanoparticles could be used to remove CO_2 from amine capture solutions, and we wanted to apply this concept as a template to explore more reactions. Specifically, our objective was to probe reactions that have a downstream product which could be monitored as a quantitative readout. We ultimately decided to implement a thermal initiator decomposition for radical polymerization.

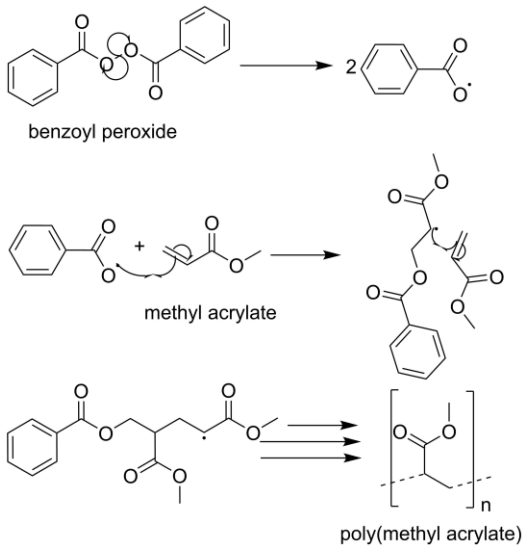

Figure 15: Reaction scheme for radical polymerization initiated by the decomposition of benzoyl peroxide

In this experiment, photothermal heating was compared with traditional bulk heating as a method to decompose benzoyl peroxide and initiate radical polymerization. Solutions of monomer and initiator are prepared with carbon black nanoparticles homogeneously dispersed by ultrasonication. The solutions are illuminated, and their temperature is monitored over the course of the reaction. The

system rapidly heats to a thermal plateau, where it stays until the thermal peak caused by autoacceleration. The temperature of this plateau is recorded and used as the setpoint for the thermal control. The autoacceleration of the bulk polymerization is chosen as the endpoint of the experiment, with the peak of the exotherm marked as the time at which the reaction is completed. Methyl acrylate was the primary monomer of interest, but both methyl methacrylate and ethyl acrylate were also tested to demonstrate the broader applicability of this system.

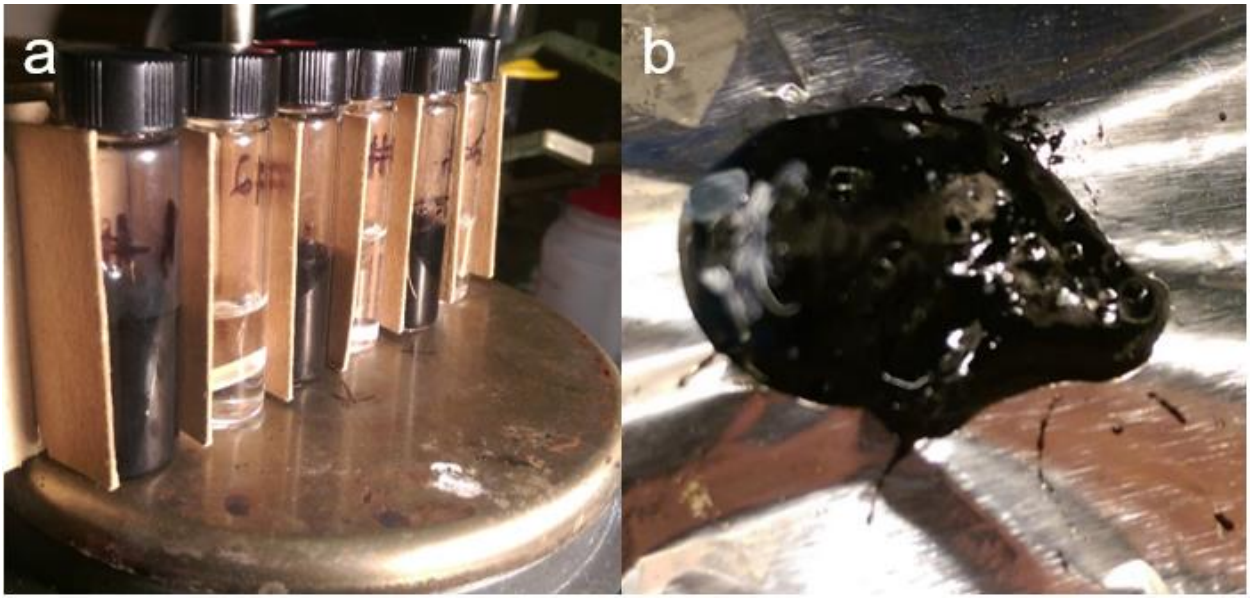

Figure 16: Pictures of a) preliminary experimental setup for photothermal polymerization and b) poly(methyl acrylate) product polymer that bubbled out of the solution vial after autoaccelleration.

2.1.2 Experimental Details

4 mL monomer solutions were prepared with 4 mg/mL benzoyl peroxide and 1 mg/mL carbon black nanoparticles, along with a small stirbar. Benzoyl peroxide concentrations were chosen based on comparable values used in literature for similar polymerizations[80], and carbon black concentrations were chosen based on previous work performed in the Esser-Kahn lab[81]. Controls are run without carbon black, without benzoyl peroxide, and without both. Solutions were capped and sonicated in a bath for 16 minutes to disperse particles. Vials were placed on a stir plate in a custom fabricated holder and stirred while thermocouples are placed into the solutions. For methyl methacrylate, the system was placed under an inert atmosphere. Thermocouples recorded the temperature while the light source was applied, and the reaction is monitored. The light source used has an irradiance of 1700 W/m^2.

[80] Co, "Free Radical Initiators."
[81] Nguyen et al., "Photothermal Release of CO2 from Capture Solutions Using Nanoparticles"; Nguyen, Stolaroff, and Esser-Kahn, "Solvent Effects on the Photothermal Regeneration of CO2 in Monoethanolamine Nanofluids."

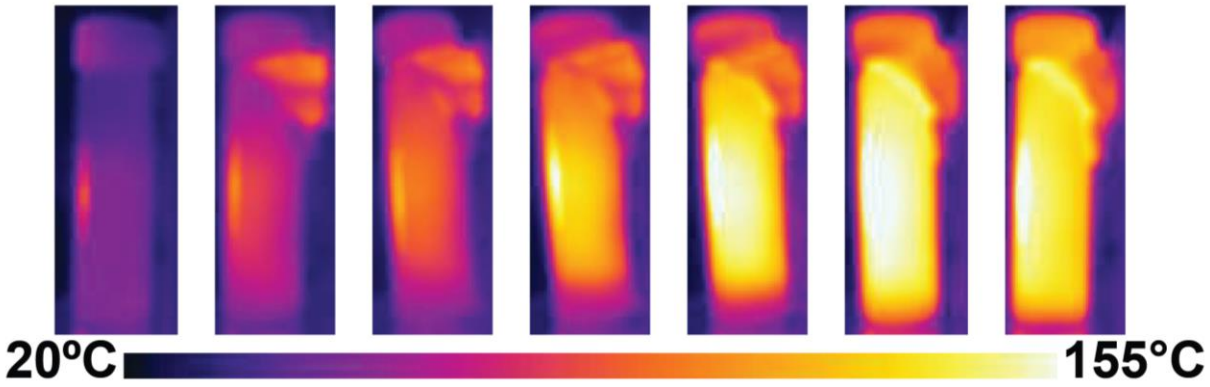

Figure 17: Thermal images taken by a Forward Looking Infrared (FLIR) camera depicting the autoacceleration point of these experiments. In the first image the solution is stirring at a stable temperature while being illuminated. Once autoacceleration begins heat rapidly evolves and the solution solidifies into a solid mass of polymer while giving off an immense amount of heat. Some polymer escapes the flask through the cap due to pressure. Time course for figure is approximately 10 s.

The reaction is monitored and eventually reaches the autoacceleration point, and the vial heats rapidly and violently, giving off steam as the polymer instantly solidifies (**Figure 17**). The peak of the thermal trace is recorded as the endpoint of the reaction. As a control, the thermal trials for methyl and butyl acrylate take the temperature recorded on the thermocouple at the onset of the light trials (56° C) and hold the reaction flask at this temperature to give a point of comparison. For methyl methacrylate, instead of holding the control at a given temperature to initiate polymerization, the no carbon black control was used, as this also polymerized after a certain time. In **Figure 18**, several characteristic thermal traces are displayed for both experimental and control groups. The autoacceleration point is obvious in both the light-based trials and the thermal controls.

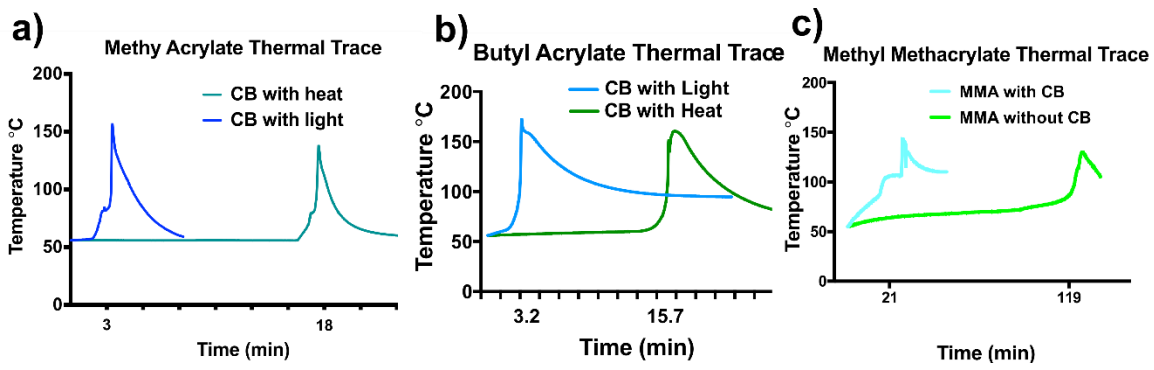

Figure 18: Characteristic thermal traces of reactions comparing the reactions that are treated by illumination and the reactions that are heated. For all three monomers the light-based system reaches its autoacceleration point well before the oil bath heated trials.

2.1.3 Results

For all three tested monomers, the time to exotherm was consistently much lower for trials that were illuminated rather than heated in an oil bath. For both acrylate monomers, the time to exotherm was less than five minutes, while for the thermal controls, the time to exotherm was more than three times as long. A similar trend held for the methyl methacrylate trials, although in this case, both polymerizations took significantly longer to reach an endpoint (21 and 119 minutes for the photothermal and control groups, respectively). These results indicate that the polymer growth occurs significantly faster in the photothermally heated reaction, even though both reaction mixtures were held at the same bulk temperature. The success of this process with multiple different monomers indicates that this enhancement is not related to the monomer used but rather to the enhancement of initiator (sition as previously hypothesized.

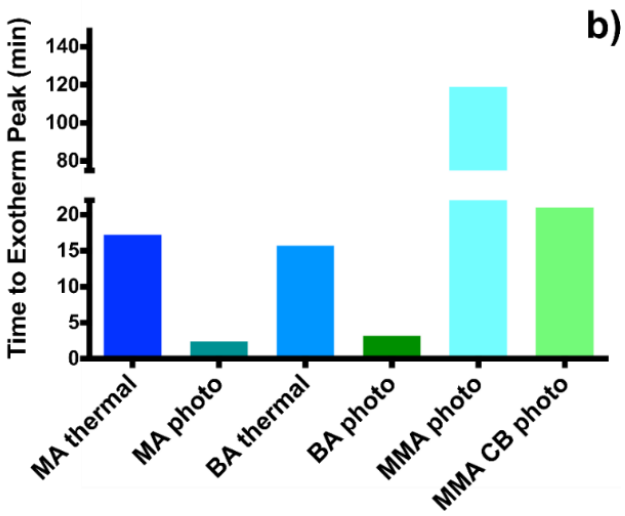

Figure 19: Bar graph depicts endpoints for various radical polymerization conditions. photo: photothermally initiated; thermal: thermally initiated via bulk heating; MA: methyl acrylate; BA: butyl acrylate; MMA: methyl methacrylate

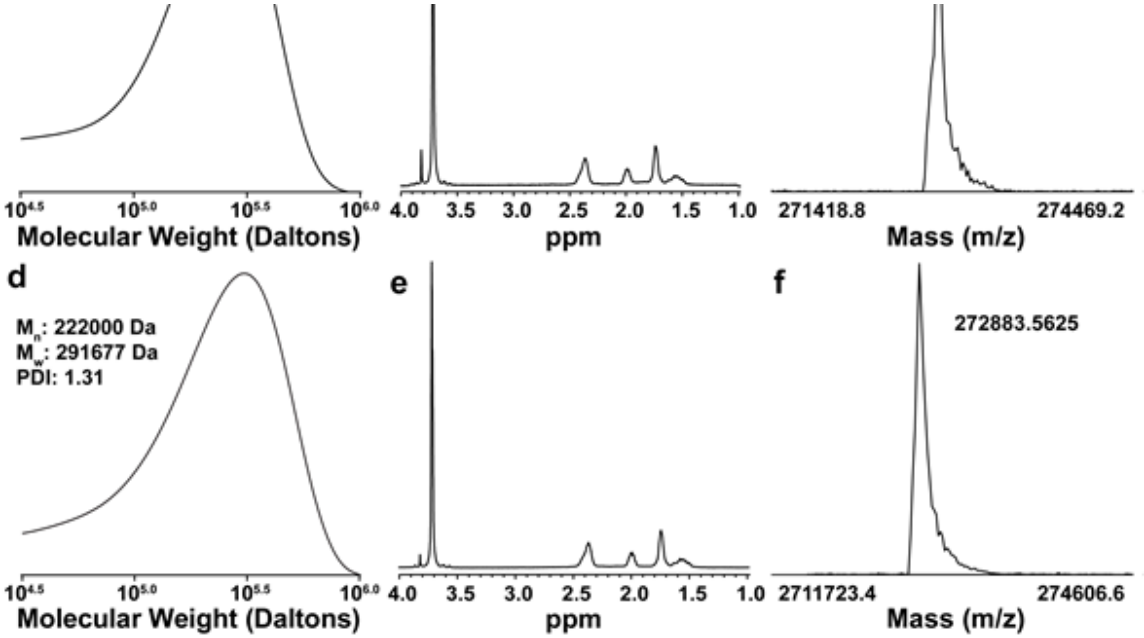

Figure 20: Graphs showing the results of analytical tests on photothermally initiated (top row) and thermally initiated (bottom row) poly(methyl acrylate). a) GPC trace of photothermally initiated methyl acrylate b) ^{1}H NMR of photothermally initiated methyl acrylate c) MALDI mass spectrum of photothermally initiated poly(methyl acrylate) d) GPC trace of thermally initiated methyl acrylate e) ^{1}H NMR of thermally initiated methyl acrylate f) MALDI spectrum of thermally initiated poly(methyl acrylate)

2.2 Characterization of Resulting Poly(Methyl Acrylate)

2.2.1 Molecular Weight Distribution

The resulting poly(methyl acrylate) polymer from both the thermal and photothermal trials was analyzed by gel phase chromatography (GPC), ^{1}H NMR (nuclear magnetic resonance) spectroscopy and MALDI-TOF (matrix assisted laser desorption/ionization – time-of-flight) mass spectroscopy, all of which are depicted in **Figure 20**. The GPC peaks were calibrated using a polystyrene standard curve. The proton NMR was used for end group analysis to validate the chemical composition of the polymers. All three tests indicated that the differently formed polymers were molecularly very similar. GPC shows very similar molecular weights and dispersity measurements. The end group integrations on the NMR are the same, indicating the similar tacticity. Visual inspection of the two spectra serve as a qualitative evaluation of chemical composition, as both the peaks and their relative ratios appear identical. The MALDI shows very close agreement again with the molecular weight between the two samples. MALDI peaks indicate the exact value for molecular weight for the most numerous polymers, whereas GPC compares to a standard curve, which may account for the discrepancy between the two measurements. The results of all three techniques indicate that the unique reaction process of photothermally initiated polymerization does not affect the core polymerization process involved and the resultant polymer is

molecularly identical to the polymer formed through standard bulk heating-based initiation.

2.2.2 Glass Transition Temperatures

Both preparations of poly(methyl acrylate) polymer were analyzed via Differential Scanning Calorimetry (DSC) to identify their glass transition temperature. DSC measurements of each sample were taken after several cycles of heating and cooling to erase the thermal history of the polymers. After analyzing the traces in **Figure 21**, the resulting glass transition temperatures were determined to be 9.4 ˚C for thermally initiated poly(methyl acrylate) and 15.7 ˚C for photothermally initiated poly(methyl acrylate). This increase in glass transition temperature for the photothermally initiated polymer is small, on the order of 5 ºC. These results, when taken together with the information about the molecular similarities of the two polymers suggest that differences may exist on the micro scale of the polymer which affect its ability to reorganize into an amorphous state.

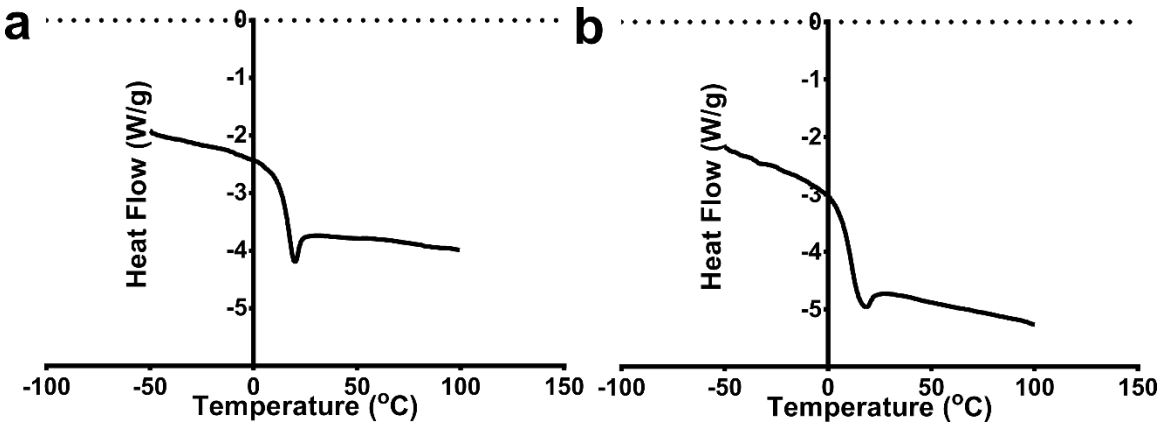

Figure 21: DSC traces of a) photothermally initiated poly(methyl acrylate) and b) thermally initiated poly(methyl acrylate)

2.2.4 Morphological Differences

Perhaps our most interesting observation was the morphological differences visible in scanning electron microscopy (SEM) images of the polymers (**Figure 22**). The photothermally initiated polymer consistently had a uniform and ordered fibrous pattern. The fibers are directionally aligned, uniform and consistent in their radii (1.16 μm ± 0.04 μm). This morphological variation was not observed in other polymers such as butyl acrylate or methyl methacrylate or for the standard thermal polymerization of methyl acrylate.; thus we concluded that this morphological artifact is specific to both the monomer, methyl acrylate, and the polymerization method of utilizing photothermal heating with carbon black nanoparticles. Different concentrations of carbon black were also examined, to identify the threshold required for the "nanofibers" to develop and to see if the morphological order varied with carbon black concentration. It was identified that that fibers appear with carbon black concentrations

as low as 0.25 mg/mL. When the concentration is increased from 5 mg/mL in the standard experiments to 20 mg/mL or 50 mg/mL as in images e) and f) in **Figure 22**, the fibrous structure is present but more chaotic and has three-dimensional organization. No mechanism or origin for this phenomenon has been identified, but we hypothesized that the fibers might be formed during the autoacceleration process, and possibly are born out of this autoacceleration "seeding" around many carbon black nanoparticles at once.

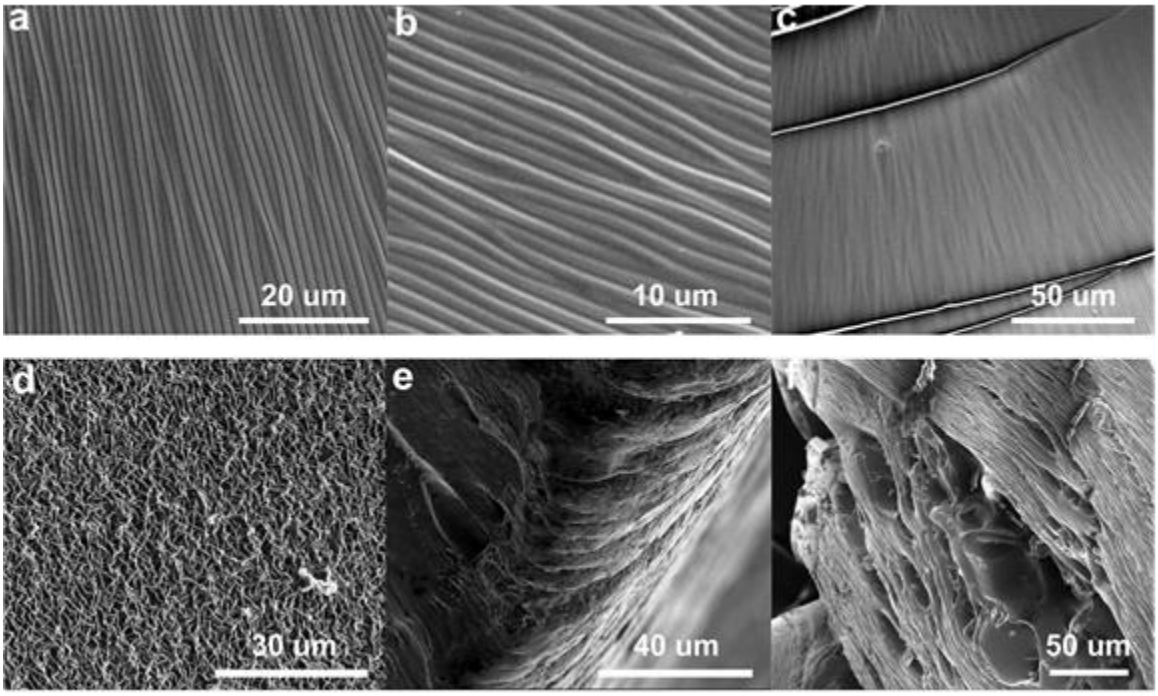

Figure 22: SEM of photothermally- and thermally-initiated polymers. (a) photothermally-initiated MA polymer at 2499× magnification; (b) photothermally-initiated MA polymer at 5000× magnification; (c) photothermally-initiated MA polymer at 850× magnification; (d) thermally-initiated polymerization at 2000× magnification; (e) lamellae of photothermally-initiated polymer with 50 mg/mL carbon black loading, 1500× magnification; (f) lamellae of photothermally-initiated polymer with 20 mg/mL carbon black loading, 650× magnification. Panels (a)–(c) show samples taken from three separate polymerization reactions.

2.3 Kinetics of Benzoyl Peroxide Decomposition in Ethyl Acetate

2.3.1 Introduction

After confirming that photothermally treated carbon black did initiate polymerization, we wanted to further confirm our process by directly measuring the decomposition of BPO outside the polymerization system. Instead of the monomer solution, BPO and carbon black were dissolved and dispersed within ethyl acetate. These samples were subsequently treated with light or heat as in the previous polymerization experiments. The concentration of benzoyl peroxide was monitored directly by high-performance liquid chromatography (HPLC) and these data were analyzed to evaluate the kinetics of the process.

2.3.2 Experimental Details

Ethyl acetate solutions with concentrations of 1 mg/mL carbon black and 5 mg/mL benzoyl peroxide were sonicated and then either heated in a thermal bath or illuminated for a set period of time. This experiment was designed to mimic the polymerization procedure to probe the rate of initiation of benzoyl peroxide in the presence or absence of carbon black. At set time points, solutions were removed from heat or illumination, then filtered and run on the HPLC to calculate the remaining benzoyl peroxide concentration. The peak at 24 minutes shown in **Figure 23** below was used to analyze the benzoyl peroxide concentration. Standard solutions of benzoyl

peroxide in ethyl acetate were used to create a standard curve based on peak area. Three replicates of nine different concentrations were used for the standard curve and then three separate trials were run for each of the photothermal and the thermal treatments with eight time points over the course of two hours.

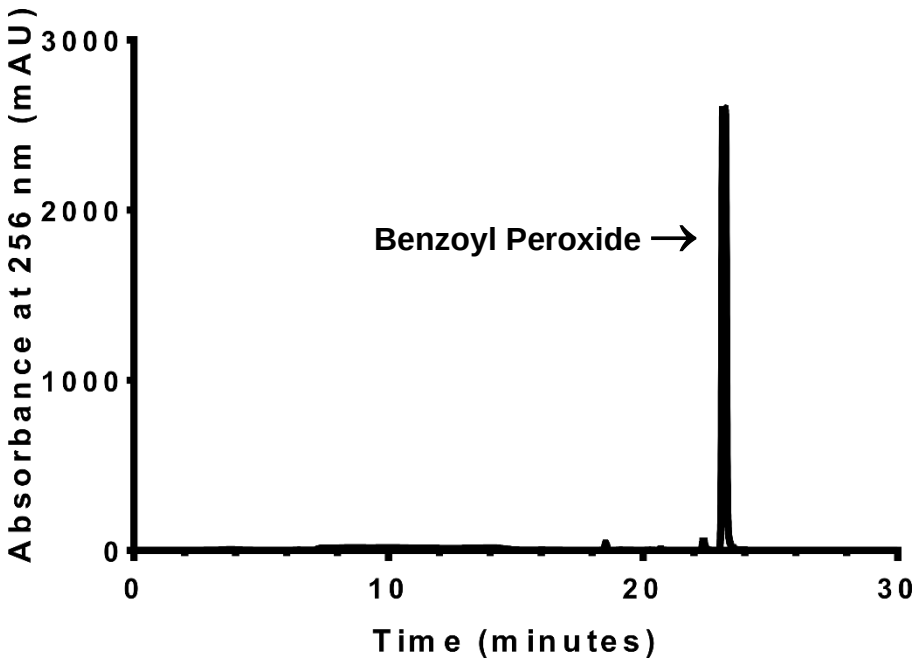

Figure 23: HPLC trace identifying the peak used to evaluate benzoyl peroxide concentration, the peak at 24 minutes was integrated and compared to a standard curve to determine benzoyl peroxide concentration

2.3.3 Results

The kinetics of photothermal heating are complex and difficult to analyze due to the unknown distribution of temperature in the reaction vessel. A current limitation was our inability to track local heating by the nanoparticles at any given time point. In particular, the concentration of benzoyl peroxide around the nanoparticles may be vastly different than in the bulk solution due to depletion from the decomposition

reactions. Because of these limitations, we examined the reaction data with some assumptions about the observable kinetics that would allow us to understand and compare them to a system without nanoscale heating. Based on data analyzing benzoyl peroxide concentration over time we concluded that the kinetics of the photothermal reactions most closely followed a first-order mechanism. We also assumed that the reaction geometry was static over the course of the experiment since the amount of carbon black, the rate of stirring and the bulk temperature were all held constant, and so the rate should only depend on the concentration of benzoyl peroxide. The thermal control allows us to compare our photothermally initiated system to a system that is initiated by bulk heating, so any increase in the reaction rate should be attributable to the nanoscale heating from the carbon black particles. The result is a pseudo-first-order rate constant (summarized in **Figure 24** b) that is an order-of-magnitude greater for photothermal heating compared to thermal heating. This confirms our earlier results indicating that photothermal heating increased the rate of reaction of the system without increasing the overall bulk temperature.

The kinetics of the reaction were analyzed assuming a first-order mechanism, but the decomposition of benzoyl peroxide is only first order at infinite dilution due to competing decomposition processes[82]. This likely accounts for the lower values for the

[82] Barnett and Vaughan, "The Decomposition of Benzoyl Peroxide. I. The Kinetics and Stoichiometry in Benzene."

coefficient of determination for the data from the thermal trials. In comparison to the thermal trials, the photothermal trials more closely follow first-order kinetics suggesting that this reaction geometry can avoid the competing processes that slow the reaction. The resulting value for the observed rate constant shows an effective temperature of approximately 90 °C, when compared to literature values for BPO decomposition[83].

a

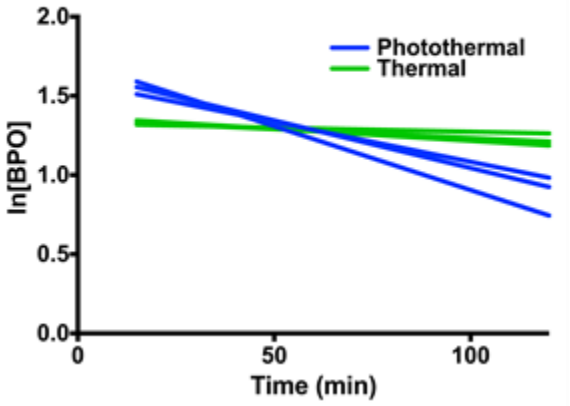

b

Rate of BPO Decomposition

Condition	k_{obs} (s^{-1})
Photothermal	$1.061 \times 10^{-4} \pm 1.487 \times 10^{-5}$
Thermal	$1.755 \times 10^{-5} \pm 4.759 \times 10^{-6}$

$$R = -\frac{d[\mathrm{BPO}]}{dt} = k_{\mathrm{obs}}[\mathrm{BPO}]$$

$$[\mathrm{BPO}] = [\mathrm{BPO}]_i e^{-k_{\mathrm{obs}}t}$$

$$\ln[\mathrm{BPO}] = \ln [\mathrm{BPO}]_i - k_{\mathrm{obs}}t$$

Figure 24: Graph depicting pseudo-first-order kinetics for both thermal and photothermal decomposition of benzoyl peroxide decomposition. a) shows the trendlines for the photothermal and thermal trials, the slope of these lines is the observed 1st order rate constant shown in b). The R^2 value for the photothermal lines ranged from 0.6316 to 0.7621 and from 0.1853 to 0.1066 for the thermal lines.

[83] Co, "Free Radical Initiators."

3.4 Conclusion

In this exploration of the power of photothermal heating to drive chemical reactions we've demonstrated that it can be used to enhance the rate of thermal decomposition for benzoyl peroxide. This enhanced reaction can then go on to drive radical polymerization of various vinyl monomers. The resulting poly(methyl acrylate) from these reactions exhibits unique morphological characteristics that suggest that the reaction geometry of nanoscale heating can introduce microstructured order to the resultant polymer in the form of fibrous structures.

The radical polymerization was activated via photothermal heating of carbon black nanoparticles. The polymerization was conducted neat, and the system was illuminated by a solar spectrum lamp at 1760 W/m^2. The reaction rate was monitored by measuring the time it took to reach the autoacceleration point of the polymerization. The photothermal systems were able to reach this point approximately four times faster than an analogous system that was not illuminated but rather kept at the same bulk temperature as the photothermal system.

Reaction kinetics of the benzoyl peroxide decomposition were examined in solutions of ethyl acetate, in order to examine the effects of carbon black in this reaction. Specifically, we wanted to isolate the initiation of BPO from the radical polymerization so benzoyl peroxide could be monitored at various points throughout the reaction via HPLC. The results showed an order of magnitude increase in reaction rate for the

photothermally heated reaction as compared to the reaction at the same bulk temperature, indicating that nanoscale heating is responsible for the bulk of the benzoyl peroxide decomposition.

We successfully probed a photothermal system for its effect on the reactivity of a high-temperature reaction. We proved that this photothermal heating was more rapid and efficient than standard bulk heating and discovered the resulting polymer has novel microstructured organization. This was an excellent first step in our exploration of novel reaction systems based on photothermal heating and gave us confidence to explore other high temperature reactions forced by photothermal heating.

Chapter 2 Bibliography

Barnett, Benjamin, and William E. Vaughan. "The Decomposition of Benzoyl Peroxide. I. The Kinetics and Stoichiometry in Benzene." *The Journal of Physical and Colloid Chemistry* 51, no. 4 (April 1, 1947): 926–42. https://doi.org/10.1021/j150454a003.

Co, Aldrich Chenical. "Free Radical Initiators," n.d., 2.

Firestone, Gabriel, Honglu Huang, Jason R. Bochinski, and Laura I. Clarke. "Photothermally-Driven Thermo-Oxidative Degradation of Low Density Polyethylene: Heterogeneous Heating plus a Complex Reaction Leads to Homogeneous Chemistry." *Nanotechnology* 30, no. 47 (September 2019): 475706. https://doi.org/10.1088/1361-6528/ab3bc0.

Fortenbaugh, R. Joseph, Sabrina A. Carrozzi, and Benjamin J. Lear. "Photothermal Control over the Mechanical and Physical Properties of Polydimethylsiloxane." *Macromolecules* 52, no. 10 (May 28, 2019): 3839–44. https://doi.org/10.1021/acs.macromol.9b00134.

Fortenbaugh, R. Joseph, and Benjamin J. Lear. "On-Demand Curing of Polydimethylsiloxane (PDMS) Using the Photothermal Effect of Gold Nanoparticles." *Nanoscale* 9, no. 25 (June 29, 2017): 8555–59. https://doi.org/10.1039/C7NR01423F.

Haas, Kaitlin M., and Benjamin J. Lear. "Billion-Fold Rate Enhancement of Urethane Polymerization via the Photothermal Effect of Plasmonic Gold Nanoparticles." *Chemical Science* 6, no. 11 (October 13, 2015): 6462–67. https://doi.org/10.1039/C5SC02149A.

Huang, Honglu, Gabriel Firestone, Daniela Fontecha, Russell E. Gorga, Jason R. Bochinski, and Laura I. Clarke. "Nanoparticle-Based Photothermal Heating to Drive Chemical Reactions within a Solid: Using Inhomogeneous Polymer Degradation to Manipulate Mechanical Properties and Segregate Carbonaceous by-Products." *Nanoscale* 12, no. 2 (January 2, 2020): 904–23. https://doi.org/10.1039/C9NR07401E.

Nguyen, Du, Joshuah Stolaroff, and Aaron Esser-Kahn. "Solvent Effects on the Photothermal Regeneration of CO2 in Monoethanolamine Nanofluids." *ACS Applied Materials & Interfaces* 7, no. 46 (November 25, 2015): 25851–56. https://doi.org/10.1021/acsami.5b08151.

Nguyen, Du T., Richard Truong, Richard Lee, Samantha A. Goetz, and Aaron P. Esser-Kahn. "Photothermal Release of CO2 from Capture Solutions Using Nanoparticles." *Energy & Environmental Science* 7, no. 8 (July 18, 2014): 2603–7. https://doi.org/10.1039/C4EE01047G.

Photothermal Heating of Nickel Nanoparticles for Conversion of Carbon Dioxide to Methane via Sabatier Reaction

3.1 Introduction

After successfully identifying another solution-based reaction where photothermal heating could drive a high-temperature process at low bulk temperatures, we decided to explore heterogenous catalysis, and examine nickel nanoparticles dispersed in the gas phase for the Sabatier conversion of carbon dioxide to methane. The spatial heating had been proven a few times over as a suitable way to create energy-efficient versions of high temperature reactions. Though heterogeneous catalysis reactions are both some of the most important reactions in industrial chemistry, they happen to be highly unoptimized, with most reactions being run at incredibly high temperatures and pressures to achieve any sort of reasonable conversion.

Shifting away from solution and utilizing the nanoparticle for the dual uses of heating and catalysis was an ambitious leap, and while successful it was not without its hurdles. Replicating the dynamics of solution-based photothermal reactions in a gas-solid system was much more complicated and a very different approach than much of the field, which begins from a catalyst science approach. The result is an exploration of this research from a completely different angle, which provides unique insight into the field that hopefully will allow it to advance.

As a disclaimer, much of this material has been adapted from a journal article manuscript that is currently being reworked for submission.

3.2 Experiments and Results

3.2.1 Initial Results

In a previous work, we determined that photothermal heating of CO_2 capture fluids with carbon black nanoparticles was sufficient to release CO_2, achieving reactivity normally observed at 120 ˚C at bulk temperatures of 60˚C[84]. In this work, we extended this idea to heterogeneous catalysis. To simplify our test system, we selected a gaseous reaction to minimize thermal transfer to the medium. We selected the Sabatier reaction for its utility – conversion of CO_2 into methane and its well documented thermal reaction profile – the production of CO and CH_4 as a function of bulk temperature. We wanted to examine if the local heating we observed in CO_2 capture solutions could be translated to the activation of CO_2 for catalytic conversion and how the lower bulk-temperatures might alter the product distribution.

In our initial experiments, we designed a simplified reactor which consisted of (1) a light source with variable intensity from 1 to 20 kW/m^2, (2) a stoichiometric mixture of Sabatier reactants (H2/CO2 4:1), and (3) nickel nanoparticles dispersed

[84] Nguyen et al., "Photothermal Release of CO2 from Capture Solutions Using Nanoparticles."

within the sealed, stirred vessel (**Figure 25**). In our initial test system, 10.0 g of nickel

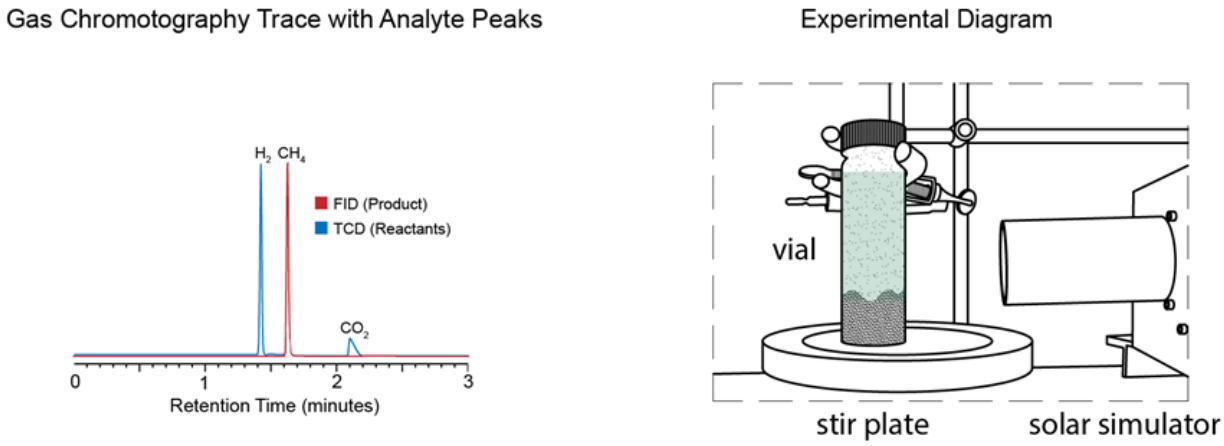

Figure 25:Photothermal Sabatier Reaction Powered by Solar Spectrum Light with Corresponding Reactant and Product Species. a) A set of example Gas Chromatography (GC) traces and b) a symbolic diagram of the reaction set-up. The two GC traces show the distribution of reactants before the reaction, as well as the distribution post-reaction, highlighting the presence of methane. Traces for both the Flame Ionization Detector (FID) and the Thermal Conductivity Detector (TCD) are shown. The experimental diagram shows the standard set-up for the experiments that follow, the green in the vial indicates where the "active" dispersed particles are in the system.

nanoparticles (99.5%, 300 nm, SkySpring Nanomaterials) were placed in a 40 mL gas sample vial. The vial was purged three times with a stoichiometric reactant mixture (H_2:CO_2 4:1). During the reaction, a positive pressure of either hydrogen or additional reactant mixture was applied via balloon. After screening different illumination levels, we observed that at an intensity of 2 kW/m^2 nanoscale heating achieved CH_4 production. At these conditions, the reactor vial temperature as measured by thermocouple never rose above 90˚C. This temperature is more than 100 ˚C below temperatures observed for other Sabatier reactions[85].

[85] Su et al., "Catalytic Carbon Dioxide Hydrogenation to Methane."

3.2.2 Light and Heat Decoupling

This surprising result led us to examine if photothermal heating of the particles was responsible. To do this, we performed several control experiments. We first tested if the bulk temperature of the reaction could be responsible on its own by heating a particle/gas mixture via an oil-bath without light. An oil bath was set at a temperature of 105°C and a vial was covered in aluminum foil to prevent light from entering. Then the system was held in equilibrium at the max temperature for the equivalent time as the test reaction. Methane production was compared to identify the difference in reactivity. We observed that the bulk temperature alone was insufficient to account for the conversion we observed (**Figure 27**, -Light Control). Next we sought to test if the particle isolation was responsible for the conversion. In this control, the reaction vial was setup in an identical fashion, but not stirred. In this control, at intensities of 2 kW/m^2, the unstirred particle control did not produce methane at measurable levels. At intensities 12 kW/m^2 and above, results were inconsistent. The reactor occasionally produced comparable amounts of methane to the light-free thermal controls and other times none. These two controls leave the most reasonable explanation as the high conversion and unique product distribution were the result of the agitated particles being heated beyond the temperature of the reaction vial during their agitation. From these experiments we conclude that photothermal heating of the particles can perform the Sabatier reaction without bulk heating of the reaction.

As an aside, this experimental technique required several rounds of refining to successfully show the decoupling. In particular, the use of a dark bath was particularly troublesome, as both water baths and oil baths appeared to overheat the system regularly, resulting in 5/20 control trials producing significant methane. This is apparent in **Figure 26**, which shows clear variability from the first 20 runs of each condition. When compared to **Figure 27**, which represents the 10 trials of each condition I did after I revised the experimental procedure, the variability of both categories is significantly reduced. The updated experimental procedure is outlined in the methods section, but the adjustments included fixing the position of the lamp and vial in a more repeatable way and using only high temperature oil for the oil bath that was equilibrated for an hour before starting the experiment.

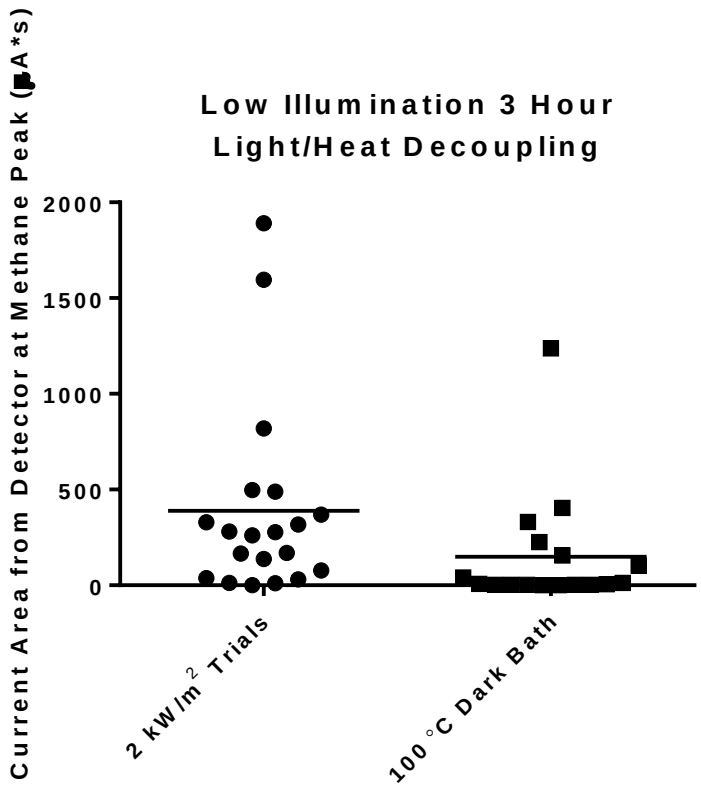

Figure 26: Initial experimental run attempting to decouple light from heat in our system. This graph represents 20 unique runs for each test condition, and Fig 3 represents 10 distinct runs done after these experiments performed with stricter experimental standards.

3.2.3 Quantifying Efficiency

While the low bulk temperature provides an interesting example for a new design of the catalytic process, for a Sabatier process, high catalytic efficiency is the most important factor. In most photocatalytic processes, high efficiency results from high intensity and subsequent high bulk-temperatures of the catalyst bed. To determine the efficiency of photothermal particle dispersions, we examined the reactivity by increasing the illumination to 20 kW/m^2. These experiments show how

photothermal heating of particles might be applied in a large-scale catalytic process, where bulk temperatures already rise to above 200 ˚C from the exothermic nature of the reaction and increased intensity. A summary of these results, as well as a comparison to our decoupled lower intensity systems, is shown in Table 2.

Table 1. Efficiencies of Several Experiments at Different Illumination Levels. Table summarizes the experimental conditions, measured methane, and resulting efficiencies for variation in time and intensity of illumination and associated controls.

Time (min)	Nickel (g)	Light Intensity	Methane (mL)	Methane (mmol)	Unadjusted Efficiency
20	10.0	12 kW/m^2	7.6	0.31	0.09 mmol/hr*g
180	10.0	2 kW/m^2	0.85	0.034	0.001 mmol/hr*g

While this process remains unoptimized, we sought to benchmark our process with reported efficiency values for photocatalytic systems. Table 2 includes a summary of our experimental efficiencies from our systems along with reported values from recent literature. As our earlier controls showed that the majority of reaction surface was on the dispersed particles, we estimated the active catalyst based on an estimate of total dispersed particles. We assumed that only the suspended particles that absorb light contributed to the reaction (based on the low light intensity previous controls). To estimate the percentage of dispersed particles, we compared the transmittance of the stirred particles to solutions of varying concentration of suspended particles with the same transmittance. Using this absorbance as a measure of particle concentration, we calculated the efficiency as a measure of mmol CH_4/hr*g of active catalyst. Given that only a small percentage of particle mass is active in the reaction process, we present this

estimate to provide an order-of-magnitude comparison to put our results in context of the field, despite the fact that these systems are supported and often heated externally.

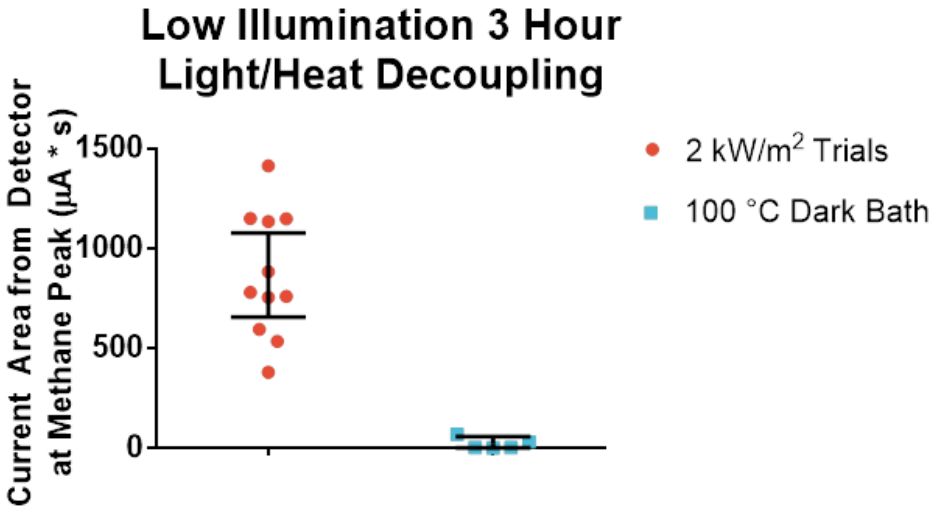

Figure 27: Comparison of Low Illumination Experimental Results and Dark Heat Control. The illuminated trials were compared to a comparable heat control, and the current area used to indicate methane production was compared system to system. The 95% confidence intervals for each treatment are graphed, and the means were determined to be significantly

3.3 Materials and Methods

3.3.1 Experimental Procedure for Illumination Experiments and Oil Bath Controls

Table 2. Comparison of Our Observed Efficiencies and Recent Literature for Methanation. Compares efficiency considering our estimate of active catalyst mass, see SI for estimation details. Note, the high temperature trial was evaluated using a different Gas Chromatography system with a different calibration.

Source	Catalyst Temperature (°C)	Light Intensity (kW/m²)	Catalyst	Catalyst Efficiency mmol/(hr*g)
This Publication	170	20	Nickel Nanoparticles	200 (estimated active catalyst)
This Publication	100	2	Nickel Nanoparticles	2 (estimated active catalyst)

Sastre et al. 2019[86]	230	10.1	Ruthenium	52
Jelle et al. 2018[87]	170	22	Ruthenium on TiO2 nanoparticles	4.4
O'Brien et al. 2018[88]	150	2.47	Ruthenium Film on inverted silicon opal crystal	2.8

In each trial a stir bar was placed inside a 40 mL gas reaction vial. The vial without the cap was tared on a scale and 10.0 g of Ni nanopowder was weighed out. Then the vial was purged with the 4:1 H_2:CO_2 gas mixture using a 50 mL syringe and two 18 G needles. The full volume of the vial was pushed through a 3" needle that blows through the particles while the other ½" needle provides pressure relief. This was repeated three times and then both needles were removed. The septa on top of the vial was then covered with fresh 5-minute epoxy mixture. This was carefully applied to cover the entire septa. After 5 min, a balloon of H_2 gas was attached to the ½" needle and pushed through the epoxy and septa. For the illumination trials, the vials were fixed in place with a clamp on the stir plate set at 1000 rpm and the lamp was placed at a set distance away calibrated to provide a set illumination to the vial. If it is a dark trial then the vial is covered in foil to block light and clamped in place in a stirred oil bath, also stirring at 1000 rpm. At the end of the trial the light is turned off or the vial is removed from the bath. At the same time the balloon and needle are both removed

[86] Sastre et al., "Sunlight-Fueled, Low-Temperature Ru-Catalyzed Conversion of CO2 and H2 to CH4 with a High Photon-to-Methane Efficiency."
[87] Jelle et al., "Highly Efficient Ambient Temperature CO2 Photomethanation Catalyzed by Nanostructured RuO2 on Silicon Photonic Crystal Support."
[88] O'Brien et al., "Enhanced Photothermal Reduction of Gaseous CO2 over Silicon Photonic Crystal Supported Ruthenium at Ambient Temperature."

from the vial. The vial is left to cool momentarily and then samples are removed via gas syringe through the septa and analyzed on the GPC.

3.3.2 Experimental Procedure for Gas Chromatography Measurements

Analysis was performed using a Agilent Technologies 7890B Gas Chromatograph (GC) System, outfitted with both a Flame Ionization Detector (FID), and a Thermal Compositions Detector (TCD). The column used is a CARBONPLOT-1010. Nitrogen is the carrier gas along with Hydrogen and Air tanks for the FID flame. For each run, a 200 μL sample is injected into the inlet, which is held at 200 °C. Gas is flowed through column at a rate of 8 mL/min for 5 min while the column is ramped up from 40 °C to 300 °C over the course of 30 seconds. Then for the next 4.5 min it is held there while gas flows through the column and out to the detectors. The FID is held at 350 °C and has 40 mL/min Hydrogen gas, 400 mL/min air gas and 10 mL/min Nitrogen gas makeup flowing through it. The TCD is held at 300 °C while 15 mL/min reference flow and 12 mL/min combined from the analyte stream of Nitrogen flow through. Each run flows through for 5 min but can be stopped early.

The methane peak was determined to be at 1.62 min via injection of a pure Methane standard from Cal Gas Direct. This peak was integrated automatically by the Agilent ChemStation software. The area of these peaks was used with the standard curve to identify the μL of Methane injected in each run. This value and the total

volume of the injection sample was used to calculate the percentage methane in each run and subsequently either the methane in the injection volume or the methane in the reaction vessel, as shown in the equations below.

$$\text{Volume of Methane in Vial} = (\%\text{Methane from Calibration Curve in S1}) * (\text{Reaction Vial Volume})$$

$$\text{Volume of Methane in Sample} = (\%\text{Methane from Calibration Curve in S1}) * (\text{Injection Volume})$$

Standards at different amounts were each injected into the system in triplicate to generate the calibration curve in Fig S1. A linear regression was performed on the data, constraining the line to begin at the origin. The R squared value was 0.9908. Values were collected for both 50 and 100 μL as well as 0.10 and 0.05 μL, but at these values the relationship was no longer linear, likely due to detector saturation and low signal-to-noise ratio, respectively.

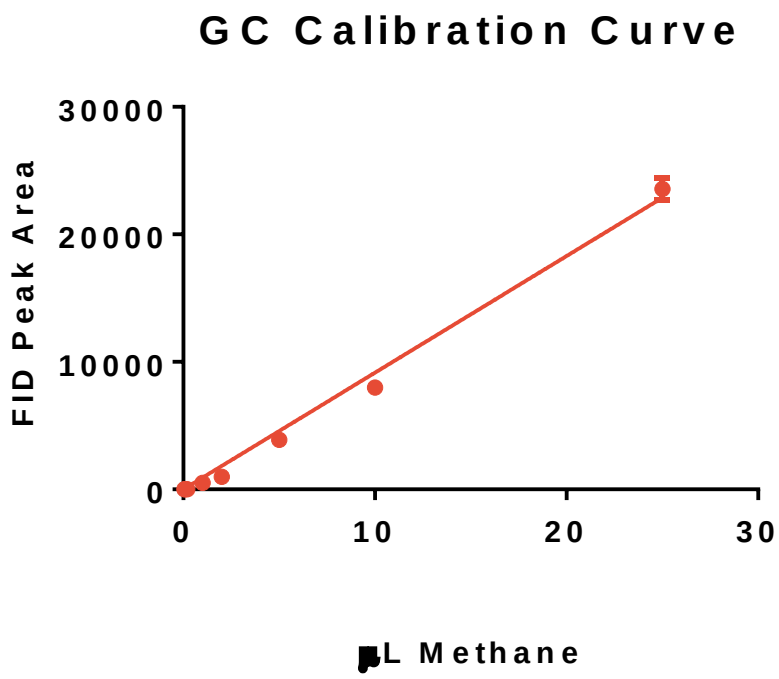

Figure 28: Calibration Curve and equation for methane using our standard method on the Gas Chromatography. Method described in detail above.

3.3.3 Measurement of "Active" Catalyst and Subsequent Calculation of Adjusted Catalyst Efficiency

A challenge in our system was estimating the "active" catalyst. Rather than using a traditionally supported catalyst, the experiments summarized here use exclusively ball-milled Ni NPs. They are dispersed in the gas mixture and isolated solely by agitation. The system, at lower temperatures, is only active when the particles are dispersed. We therefore wanted to do a mathematical estimation of "active" Ni catalyst at any given point. In the **Figure 29**, we describe how we used measured the absorbance

for different concentrations of Ni NPs in water to create a Beer's Law equation. With this equation we estimated the active catalyst in the reaction chamber to be 0.13 g/L. By assuming our catalyst, when dispersed, follows the same absorbance rule, we calculated that for a 40 mL reaction chamber filled with 10 g, we have 5.3 mg of active catalyst at any time during the reaction. To estimate an active catalyst amount to provide comparison to other similar systems, we therefore used the adjustment ratio of 2000:1 for active catalyst efficiency.

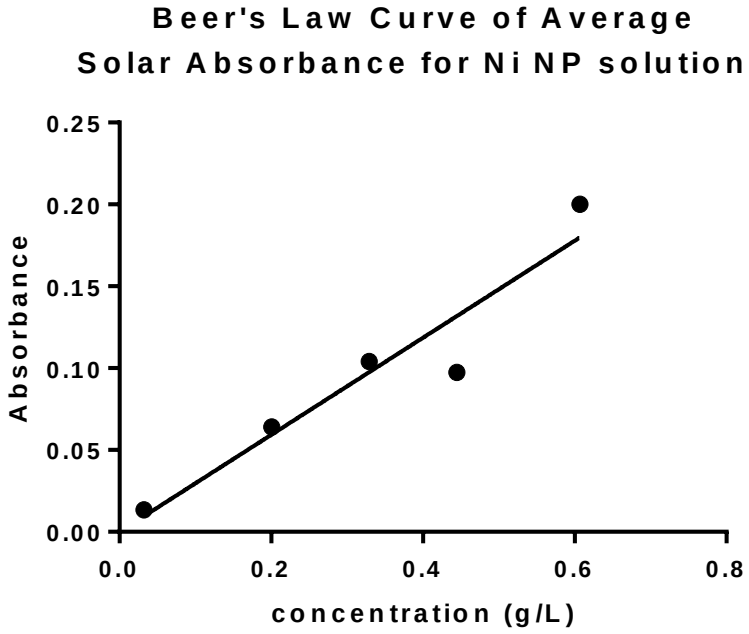

$$\text{Absorbance} = 0.2964 \times 1\text{cm} \times \text{Concentration (g/L)}$$

Figure 29: Beer's Law Plot for Ni NP solutions in water. The absorption of light in the solar spectrum for these water Ni solutions was compared to the absorption of light for the reaction chamber to estimate the active proportion of catalyst as described above. The Beer's Law equation is below the graph, the R squared value is 0.91. The estimated concentration inside the vial is 0.13 g/L, factoring in the 2.7x increase in path length from the cuvette to the reaction vial.

3.3.4 Collection of BET Adsorption Isotherms to Determine Available Catalytic Surface Before and After Experimenting

Brauner-Emmet-Teller (BET) analysis and experiments were performed using a Micrometrics 3-Flex system. Samples were weighed out on a high precision (Δ0.1 mg) scale and placed in the analysis chamber. The system was cooled using liquid nitrogen to -196 °C and pumped down to 7 mmHg, the gas used for analysis was N_2, and each sample was taken through one full cycle of adsorption and desorption as shown in **Figure 30**. A sample of particles fresh from an unopened bag of Ni nanodust were analyzed, a sample from a bag that that had been left exposed to atmosphere, and from a set of particles that had been used to successfully produce methane in an experiment.

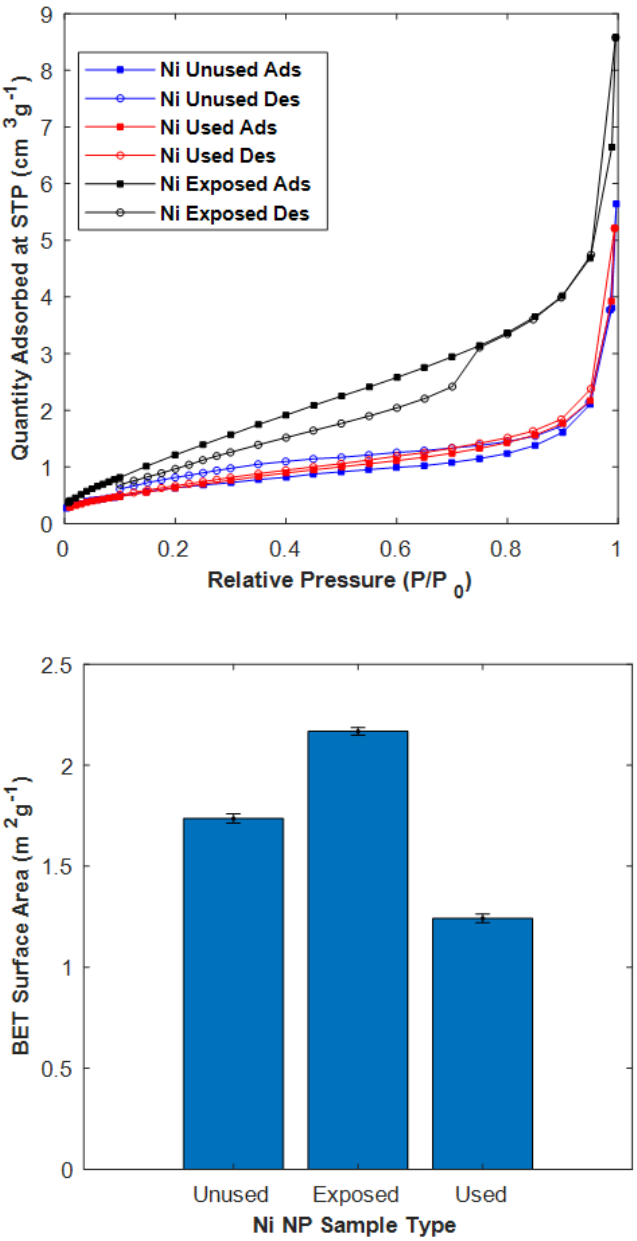

Figure 30: Summary of BET Adsorption Data for Ni NPs comparing particles after a photothermal catalysis procedure, prior to any light of gas exposure, and prior to light exposure, but exposed to ambient atmosphere. Particles exposed to the atmosphere have slightly higher surface area implying that the surface may be slightly altered by exposure to the atmosphere. Used particles then seem to decrease in surface area, indicating that some of the catalyst surface may be altered or poisoned.

3.4 Conclusion & Future Exploration

In conclusion, we identified photothermal heating of unsupported nanoparticles dispersed in a gas mixture as a method for heterogeneous catalysis processes that require high temperatures. Our test system uses the Sabatier reaction on nickel nanoparticles. By tuning the illumination level, we controlled the bulk temperature and reactivity of our system. In low irradiance, reactivity derives solely from nanoscale heating. At higher irradiances closer to focused light applications, high overall efficiency was achieved over a thermal only control – indicating improved yield from photothermal catalysis. This system has the benefits of being cheap and simple, and combined with traditional catalysis science, it may be possible to develop a supported, suspendable, nickel nanoparticle-based industrial catalyst for industrial methanation.

The photothermal Sabatier reaction has been well demonstrated but implementing the process in an actual reactor that illustrates how such a system would be run is the important next step. Shaping of light sources and suspension of nanoparticles would be important to optimizing this process, and someone with expertise in industrial reactor design would be ideal. Another option would be to try other reactions, such as the Haber-Bosch process or the epoxidation of ethylene.

Chapter 3 Bibliography

Jelle, Abdinoor A., Kulbir K. Ghuman, Paul G. O'Brien, Mohamad Hmadeh, Amit Sandhel, Doug D. Perovic, Chandra Veer Singh, Charles A. Mims, and Geoffrey A. Ozin. "Highly Efficient Ambient Temperature CO2 Photomethanation Catalyzed by Nanostructured RuO2 on Silicon Photonic Crystal Support." *Advanced Energy Materials* 8, no. 9 (2018): 1702277. https://doi.org/10.1002/aenm.201702277.

Nguyen, Du T., Richard Truong, Richard Lee, Samantha A. Goetz, and Aaron P. Esser-Kahn. "Photothermal Release of CO2 from Capture Solutions Using Nanoparticles." *Energy & Environmental Science* 7, no. 8 (July 18, 2014): 2603–7. https://doi.org/10.1039/C4EE01047G.

O'Brien, Paul G., Kulbir K. Ghuman, Abdinoor A. Jelle, Amit Sandhel, Thomas E. Wood, Joel Y. Y. Loh, Jia Jia, et al. "Enhanced Photothermal Reduction of Gaseous CO2 over Silicon Photonic Crystal Supported Ruthenium at Ambient Temperature." *Energy & Environmental Science* 11, no. 12 (December 5, 2018): 3443–51. https://doi.org/10.1039/C8EE02347F.

Sastre, Francesc, Caroline Versluis, Nicole Meulendijks, Jessica Rodríguez-Fernández, Jorgen Sweelssen, Ken Elen, Marlies K. Van Bael, Tim den Hartog, Marcel A. Verheijen, and Pascal Buskens. "Sunlight-Fueled, Low-Temperature Ru-Catalyzed Conversion of CO2 and H2 to CH4 with a High Photon-to-Methane Efficiency." *ACS Omega* 4, no. 4 (April 30, 2019): 7369–77. https://doi.org/10.1021/acsomega.9b00581.

Su, Xiong, Jinghua Xu, Binglian Liang, Hongmin Duan, Baolin Hou, and Yanqiang Huang. "Catalytic Carbon Dioxide Hydrogenation to Methane: A Review of Recent Studies." *Journal of Energy Chemistry* 25, no. 4 (July 1, 2016): 553–65. https://doi.org/10.1016/j.jechem.2016.03.009.

Finite Element Modeling to Understand Spatial Reaction Dynamics

4.1 Introduction

While completing the two main projects of my thesis, I was also drawn to the spatially unique reaction systems present in my colleagues' work. I offered my expertise with finite element modeling (FEM) via the COMSOL software in order to provide context for and back up the work present in their projects. While this work was a diversion of photothermal heating, it was a diversion that gave me the chance to contribute my thoughts and energy to other projects that explore different spatial reaction dynamics.

In section 1.2, I highlight the work I've done recently to model the self-strengthening of a dynamic polymer system. This system is based on a novel gel that strengthens in response to mechanical stretch due to piezoelectric -activated crosslinking reactions. This system was borne out of previous work that used ultrasonic activation, with this system taking the next step to activate polymerization via acoustic frequency mechanical oscillation. My work models how the unstrengthened gel responds to these oscillations based on the gel geometry, identifying the spatial distribution of stress across the material.

In section 1.3, I modeled the chemical transport dynamics for a microfluidic reactor that utilized an upconversion system to generate singlet oxygen for the

conversion of α-terpinene into ascaridole. My model took the known values for rate constants, flow rate, and reactor geometry to generate values for α-terpinene conversion based on singlet-oxygen generation rate. We could compare these values for conversion with the experimental model to identify an estimation for the singlet oxygen generation within the reaction. This allowed for validation of the system's ability to generate singlet oxygen at a certain rate and decouple the results from the effects of running it in a microfluidic reactor.

Both projects drew me further into the world of exploring spatial reaction dynamics from a computational angle, and the results were helpful to both projects. As a disclaimer, some of the material in this chapter has been adapted from or reproduced from the relevant publications, including a pre-submission version of the dynamic self-strengthening paper.

4.2 Finite Element Modeling of Dynamic Self-Strengthening Polymer System

4.2.1 Objectives of Model Dynamic Self-Strengthening Polymer System

At the point where I entered the project, my colleagues had successfully managed to create a gel system that self-strengthens via cross-linking triggered by sonic frequency oscillations. After treatment, the strengthening of the material showed distinctive patterning, with some parts growing stiffer than others in terms of their Young's moduli.

My role was to build a COMSOL model of the starting gel and identify a time-averaged stress map over the course of many oscillations. The resulting stress map should give a clear indication of which parts of the material received the most stress, at least initially. The experimental results can be compared to these computational stress patterns, and it can be indicated how important the initial stress experienced by the material is to the resulting strengthening.

4.2.2 Methods

Simulation was performed in COMSOL Multiphysics® 5.4 using the Solid Mechanics module and a Time-Dependent study. The material was simulated as a Linear Elastic Material with the bottom and sides subject to the 2000 Hz oscillation and the top of the cylinder left free. The inputted density was 1.116 g/mL, the Young's modulus 3000 Pa, and the Poisson's ratio was 0.4999. The oscillation was implemented via a Prescribed Acceleration that applied to both the sides and bottom of the cylinder; the only nonzero input was a harmonic perturbation in the z-direction that was inputted as -8[m/s2]cos(2000[Hz]*t), where t is in seconds. This corresponds to the measured amplitude of oscillation of 2 μm for a standard experimental sample. A "Finer" mesh was selected, and the system was simulated from t = 1 to 1.5 s with timepoints of 1 ms. The last 450 timepoints were averaged together to form the time average displayed in **Figure 31** D. For the simulation shown in **Figure 31** E, the settings were the same except the acceleration was applied to only the bottom of the cylinder.

The cylinder dimensions were set as a radius of 0.5 cm and a height of 1.3 cm. The cuboid sample has a dimension (cm) of 1.8 x 0.7 x 1.3. The triangular prism at the middle has a length of one side of the triangle to be 0.6 cm. The acceleration was also applied to only the bottom of the cylinder.

4.2.3 Results

Figure 31 below is the presubmission figure for upcoming publication on this work and visually compares the models with their experimental counterparts. In each case the simulated stress map shows interesting similarities and differences with the experimental stress measurements. B and E seem to be almost inverted in the vertical distribution of their stress. This suggests that while these initial strengthening patterns are relevant for the first stage of strengthening, the oscillations rapidly alter the geometry and stress map of the system, so the resulting systems then undergo different stress extrema in different places.

A future option for these experiments is to oscillate them for much shorter periods of time and analyze the crosslinking at different time points. This would allow us to update our model to be iterative, where we essentially build our own finite time series that shows where the new stress in each system is.

In **Figure 32**, I highlight more detailed Von Mises stress maps for the geometries in **Figure 31**, as well as some predictive geometries I tried out to see how their stress

maps presented. An important distinction both here and in **Figure 31** is that it matters whether the gel is within a vial. Assuming the gel is not sliding on the glass, that means that the oscillation of the system is being applied as a shear force on the sides. We both modeled a system within and without a vial as well as examined the experimental version. Pairs A & D and B & E show this off very well. Morphological differences are extreme, and in the case of A, the sides appear to create an internal region of very low cross-linking. In the future we'd like to examine experimental versions of C and D in **Figure 32**, to see if this model holds up in that case.

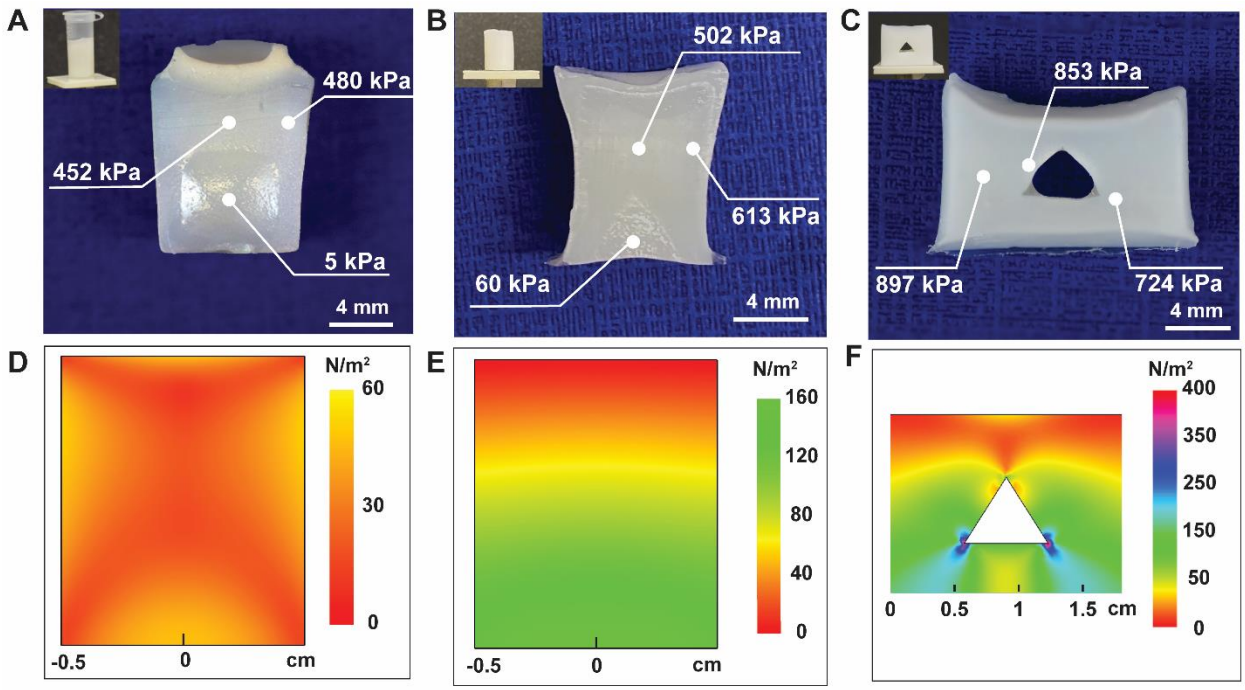

Figure 31: (A-C) Photographs of the longitudinal section of the gel samples of different geometries obtained after vibration (2000 Hz, 1.2 N, 13 h). The elastic modulus at test locations were labeled in the photographs). The inserted photographs show the different gel samples mounted on the electrodynamic shaker. (D-F) Finite element simulation via COMSOL Multiphysics® 5.4 of Von Mises stress distribution of longitudinal section of the corresponding samples oscillated at 2000 Hz. Material parameters were assumed spatially uniform and elastic.

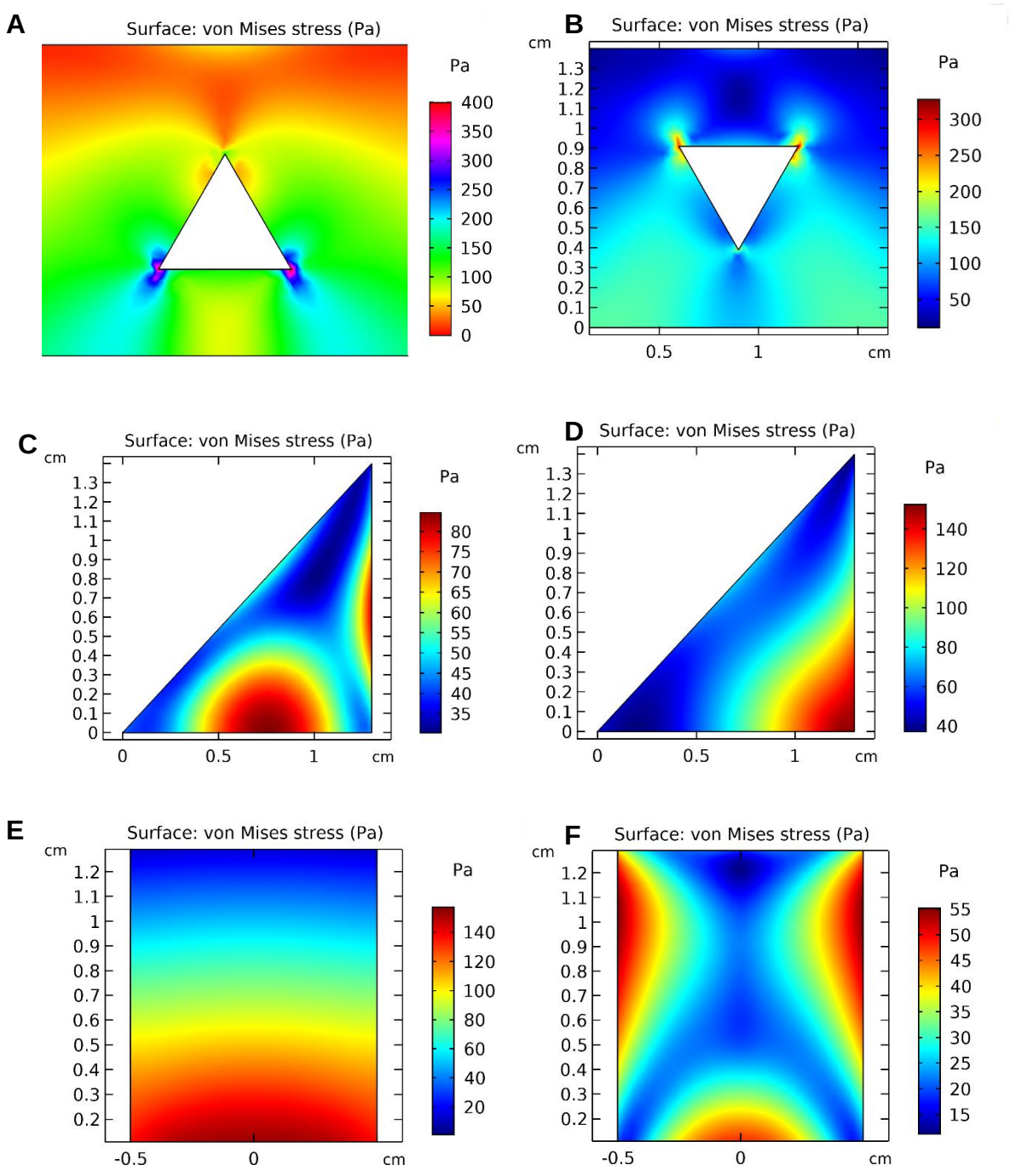

Figure 32: Von Mises Stress Maps in their own scale to show detail. A, E, and F are the same simulations of from Figure 1, whereas B is an alternate inverted triangle punch out system, and C and D are both cubic systems that have been sliced along the diagonal. C and F have the sides fixed as part of the oscillation, simulating the system being inside a vial while being oscillated, whereas D and E are free, with only the bottom moving.

4.3 Finite Element Modeling of Ascaridole Upconversion Microfluidic Reactor

4.3.1 Objectives of Model

The experimental system was a 6 cm microfluidic test reactor, through which a α-terpinene methanol solution was combined with pure oxygen in a slug flow reactor. Slug flow is when two different solutions or gases are alternately pushed through the reaction system. Light was shown through polymer block in which the microfluidic system was embedded, where it was upconverted by the upconversion system within the polymer. The upconverted light generated singlet oxygen in the solution via interaction with $[Ru(bpy)_3]^{2+}$ ions, which then reacted with the α-terpinene to generate ascaridole. The generation of singlet oxygen is a photochemical process, relying on both the concentration of dissolved oxygen as well as the incident light. However, if we assume that the methanol is saturated with oxygen due to the slug flow nature of the reaction, the kinetics of the system can be greatly simplified, as the generation of singlet oxygen can be reduced to a pseudo-first order reaction. The reaction scheme below shows this reduced reaction dynamics.

$$[O_2] \xrightarrow{h\nu + [Ru(bpy)_3]^{2+}} {}^1[O_2] \quad (1)$$

$${}^1[O_2] + [\alpha\text{-terpinene}] \longrightarrow [\text{ascaridole}] \quad (2)$$

Equation 1: Simplified reaction scheme for ascaridole conversion within the microfluidic reactor.

Diffusion rates for each of the reactant and product species is known, as well as the rate constant for the conversion of α-terpinene and singlet oxygen into ascaridole. In the experimental system we could control the flow rate, the starting concentration of α-terpinene, the incident light, and the temperature. We could then measure the concentration of ascaridole in the end product. I needed to build a reactor that took these parameters, the geometry of the system, and allowed us to identify an estimate of our singlet oxygen generation rate. To do this, I simulated a continuous flow system with singlet oxygen constantly being generated. We ran the model at the same flow rates as experimental runs and iteratively modified the rate constant for singlet oxygen generation. In this way we were able to determine an "effective" rate of singlet oxygen generation for the system.

$$\frac{d^1[O_2]}{dt} = k_1 - k_2{}^1[O_2][\alpha\text{-terpinene}]$$

$$\frac{d\,[\alpha\text{-terpinene}]}{dt} = -k_2{}^1[O_2][\alpha\text{-terpinene}]$$

$$\frac{d\,[\text{ascaridole}]}{dt} = k_2{}^1[O_2][\alpha\text{-terpinene}]$$

Equation 2: Differential equations dictating reaction concentrations. Since k_2 is known, and the initial concentration of α-terpinene is set, these equations can be inserted into the model along with a guess of k_1.

4.3.2 Methods

The COMSOL model simulating our reactor design was designed with an idealized geometry and simplified reaction kinetics. We assumed a methanol solution

constantly saturated with O_2 at all points in the system and did not simulate our actual slug flow design. We assumed singlet oxygen generation to be a constant process in an illuminated system and used our experimental results to derive pseudo rate constants for both the generation of singlet oxygen and its addition to α-terpinene to produce ascaridole. We confirmed our experimental parameters with multiple trials with a variety of modifications to experimental parameters.

4.3.3 Results

Both the model and the experiments showed that slower flow rates (and thus longer residence times) were associated with higher conversion[89]. Although our model predicts 100% conversion which we did not see in our modified reactor design. The assumption of saturated methanol may be to blame, as slug flow may result in some parts of the solution being depleted as the reaction continues. Flow systems intended for field or industrial use could be designed within this model to help maximize conversion and throughput.

[89] Wu et al., "Photon Upconversion for the Enhancement of Microfluidic Photochemical Synthesis."

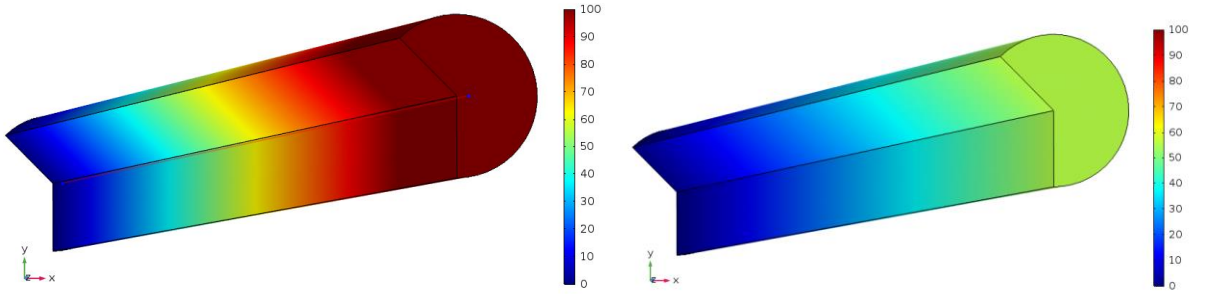

Figure 33: Side-by-side of a reactor simulation going to 100% completion (A), and another reactor going only to 60% conversion (A), based only a difference in simulated singlet oxygen generation. The length of the reactor is ~ 6 cm and the radius is ~1 mm

In **Figure 33**, the systems simulated are identical except for the pseudo zeroth order rate constant for singlet oxygen generation. Flow rate changes the conversion, as in the actual system, however the actual system never reaches 100% conversion, generally maxing out at 80%. Slug flow may have limited the diffusion of the reactants, or possibly the ascaridole-rich solution did not take up oxygen as well.

4.4 Conclusion

Computation, in tandem with experimental confirmation, gives us insight into whether our understanding of the physical and chemical behavior within a system is accurate. In the dynamic remodeling project, our model gave us confirmation that the stress on the gels was unevenly distributed and guided our hypothesis that the stress throughout the system is altered by early crosslinking. In the microfluidic reaction, our model was able to give us a good estimation for our singlet oxygen generation rate constant, as well as insight that the lack of total conversion was not a rate issue, but

likely due to changes in oxygen solubility or the limitations of slug flow chemical transport.

Chapter 4 Bibliography

Wu, M., B. A. Moser, T. M. Steeves, A. Figueroa, B. M. Wallace, S. T. Kim, A. P. Esser-Kahn, and R. C. Steinhardt. "Photon Upconversion for the Enhancement of Microfluidic Photochemical Synthesis." *RSC Advances* 9, no. 45 (2019): 26172–75. https://doi.org/10.1039/C9RA03468D.

Conclusion

Photothermal heating for high temperature reactions was exciting four years ago when I began my research, and the work I've completed since then leaves me very excited for the future of the field. The use of these systems in the toolkit of polymer chemists and engineers means it's likely to find deeper uses as time goes on. And the amount of innovation of catalysts and reaction systems in the methanation field astounds me. I believe the work that I've completed on a simple nickel system might allow for the translation of this and other photothermal systems into industrial use someday; hopefully in a plant capturing CO_2 and reforming it back into fuel utilizing solar energy.

For the future investigators working on these problems, I encourage you to reach out to everyone you can for assistance, including myself. I encourage you to chase down ideas that excite you, and to then work on building up the expertise to support your interest.